097158

2018 Geophysical Assessment Report on

Golden Horseshoe Property

Tatlemain Lake area, north of Carmacks; NTS 115I 09

Location: Latitude of 62° 31' 53.32" N, and Longitude 136° 15' 59.76" W

Halo 17 (YF50057) to Halo 60 (YF50100),

Halo 61 (YF50415) to Halo 210 (YF50564),

and Halo 211 (YF52021) to Halo 266 (YF52076)

Owner: Thi My Linh Pham

Mining District: Whitehorse

Yukon Territory

Prepared By

Nicolai Goeppel, Higher Ground Exploration Services

July 12, 2018

Work Performed from:

July 4, 2018
to
July 5, 2018

Abstract

The Golden Horseshoe Property covers 250 quartz claims in central Yukon, approximately 50 km north of Carmacks and 20 km east of the Klondike Highway and power. Claims include Halo 17 (YF50057) to Halo 60 (YF50100), Halo 61 (YF50415) to Halo 210 (YF50564), and Halo 211 (YF52021) to Halo 266 (YF52076). The property was staked based on the presence of a large elliptical geophysical anomaly in regional first vertical derivative with associated elevated gold in regional stream sediment samples. Based on the recorded porphyry and intrusion related mineralization to the immediate southwest, the anomaly was interpreted as potential pyritic contact halo to potential porphyry. In 2016 a small drilling program was undertaken to test the porphyry potential; however due to cold weather conditions the drilling only reached 375m from the desired 600m. Analytical results did not produce any anomalies, yet significant alteration was observed as potassic alteration and as several oxidized and clay altered horizons.

In 2018 an airborne magnetic and radiometric survey was completed by Precision Geophysics. Results indicate the presence of a substantial intrusive body or ring dyke complex associated with an intrusion; the geophysical signature is characteristic of large porphyry deposits and warrants further work. The total assessment valuation for 2018 work is...

Table of Contents

Introduction

The Golden Horseshoe property (GHP) lies southeast of Tatlmain Lake, north of Carmacks at the center of the Yukon (Figure 1). The property lies approximately 50km southeast of the operating Minto Mine a deformed alkaline Cu-Au porphyry with a sulphide resource of 70.8 Mt grading 1.2 % Cu, 0.5 g.t Au and 4.2 g/t Ag (Mercer and Sagman, 2012). Approximately 50 Km to the southwest is the Freegold Mountain area, a hot bed of porphyry and intrusion-related mineralization; deposits include, Tinta Hill (intrusion related vein), Revenue (Cu, Au, Mo porphyry), La Forma (high-sulphidation epithermal), and Guder (Au skarn). The closest significant mineralization is 30 km to the southwest; the Copper North porphyry supergene deposit which as of 2016 has an indicated and measured resource of 15.69 million tonnes oxide ore grading 0.94% Cu and 0.38g/t Au.

The Golden Horseshoe property overlies the early Jurassic McGregor pluton (Figure 6). In 2012 the author noted a large horseshoe shaped geophysics anomaly in the area underlain by the McGregor pluton. The first vertical derivative regional airborne magnetics anomaly displays an open-ended ellipsoidal magnetic high and central magnetic low that is approximately 9km x 14km in size (Figure 3 to 5). Based on the close proximity to existing porphyry mineralization, the horseshoe anomaly may be indicative of a pyritic contact halo to a buried intrusion. Government regional stream sediments samples from the McGregor pluton display multiple over 50 ppb gold-in-silt anomalies (Figure 2).

In 2018, Precision Geophysics was hired to conduct an airborne magnetic and radiometric survey was flown over the Halo claims in order to better target further work and future drilling. The survey results indicate the presence of a substantial intrusion or ring dyke complex associated with an intrusion. Such elliptical anomalies are characteristic of large porphyry deposits. The purpose of this report is to summarize the assessment work carried out in 2018 on the Golden Horseshoe property. The total assessment valuation is $...

Location and Access

The Golden Horseshoe project area is located in central Yukon, in the Whitehorse Mining District, and NTS map sheet 115I 09. A total of 250 quartz claims make up the project and are all in good standing (see Figure 9 for complete claim list). The GHP is centered on latitude 62° 31' 53.32" N and longitude 136° 15' 59.76" W. The project lies approximately 50 km north of Carmacks and approximately 20 km east of the Klondike Highway and power (Figure 1). Specifically, the project is area is largely below treeline and ranges in altitude from 700-1250 m. Old burn is common through the area. Primarily gently undulating hills with castellated ridge tops reveal minimal exposure below treeline. Nearby infrastructure makes for cost-effective exploration on the property and good feasibility if any significant discoveries are made.

Previous History

Industry-related

Despite substantial exploration to the west side of the Yukon River (~30-50km away) that has lead to the determination of several porphyry deposits and the active Minto mine, very little recorded exploration work has occurred in the Golden Horseshoe property area and underlying McGregor pluton. The Tatlmain occurrence 115I 114, is located approximately 3km east beyond the Horseshoe anomaly. In August 1986 Noranda Exploration Company Ltd, staked the "Main claims" to cover a RGS sample that yielded 141 ppb Au, 99 ppm As, 1160 Ba, 4 ppm Mo, and 3.8 ppm Sb. The short exploration program consisted of follow up silt samples, panned heavy samples, soils and one rock sample. Soil samples produced 770, 70 and 90 ppb Au, 1.8 ppm Ag, 24 ppm As, 68 ppm Cu, and 98 ppm Zn. Silts returned up to 4 ppm Sb and panned silts returned 1600 ppb Au and 560 ppm Zn.

Approximately 20km southeast of the GHP area is the Cu, Au alkaline porphyry Oobird occurrence. Discovered but not staked in 1971 by Laberge Joint Venture. Records mention traces of chalcopyrite and bornite occur with 5 to 20% pyrrhotite and pyrite on the margin of a hornblende-feldspar porphyry dyke cutting a hornblende-syenite batholith of Cretaceous age.

Recent Work

In late summer of 2014 Maurice Colpron, Patrick Sack, MDRU professor Murray Allen, and the author Nicolai Goeppel set out on separate traverses through the McGregor pluton region by helicopter. The 2014 traverse by the author covered approximately 10 km of the western arm of the geophysical anomaly which also makes the most prominent ridge in the area before the anomaly curves into the valley bottom near Tatlmain Lake. The goal was to cover as much area as possible with the best likelihood for rock exposures in the one-day visit and to look for confirming evidence to suggest porphyry mineralization, specifically a pyritic halo. Most notable observations showed granite to be of similar composition and grain size as at surrounding mineralized areas a porphyritic hornblende/biotite granodiorite. The medium-fine to medium grainsize suggests mineralized horizons if present are intact. Stacking of biotite suggest recrystallization. Soft chloritized and locally sericitized mafic minerals where also observed. Several areas exposed red oxidized soils and slightly limonitic porphyritic granodiorite. Six rock samples and 3 soil samples were collected.

Assays returned elevated Cu (up to 17ppm), two with elevated Ti (>0.1%), strongly elevated V (202ppm), P (930ppm), Ba (220ppm), Sr (160ppm), Rb (33ppm), slightly elevated Pb and Zn in most samples (Figure 6). Typical Cu porphyry systems contain elevated Cu, Ag, Au and also Ti, V, P, F, Ba, Sr, Rb, Nb, Te, Pb, Zn, REEs and PGEs as mineralization pathfinders. Soil samples returned: 13, 5, and 11 ppb Au; 0.19 ppm Ag; 22 and 24ppm Cu, 102.5 ppm Zn and anomalous V, Ba, and REEs. Anomalous values are encouraging, as based on geophysical interpretation, the transverse was along the pyritic halo rather than across the mineralized core. Furthermore, as the anomaly coincides with the ridge a strong response would be expected; however, the anomaly remains strong to the north where it dips 500 meters lower through the valley and would be buried beneath thick overburden. This would infer that the anomaly represents something much deeper.

In fall of 2016, a 375m diamond drilling program was carried out on the Golden Horseshoe property. The hole location, depth and azimuth are tabulated below. Supplies and equipment were hauled to a staging location north of Carmacks, off of the Klondike Highway. An A-star helicopter was used to transport equipment and supplies approximately 25 kilometers to the drilling location. A 4-person drilling crew and 2-person prospecting team where dropped onsite with drill from 28th of September, 2016 until the 6th of October, 2016. Drilling completed 375m of the intended 600m before cold weather forced an end to the program.

Drill core was flown out by helicopter to staging where it was then trucked to the Whitehorse core library where it was logged and prepared by Higher Ground Exploration Services. Core submitted for assay was brought to the ALS prep facility in Whitehorse. Analytical tests were conducted by ALS Global in Vancouver, BC, which is ISO accredited. Samples are crushed to 70% less than 2 millimetres, and a 250-gram sample is split with a riffle splitter. The split is pulverized to 85 per cent less than 75 microns, and 30 gram charges go through a multi-element assay with ICP-AES finish. Samples with gold, silver, copper, lead, or zinc exceeding the upper detection level are reanalyzed with ore grade determinations that are deemed most appropriate by the lab. Rigorous procedures are in place regarding sample collection, chain of custody and data entry. Certified assay standards, duplicate samples and blanks are routinely inserted into the sample stream to ensure integrity of the assay process.

Regional Geology

The Golden Horseshoe property area lies within the Intermontane Belt, which in the Carmacks map-area is separated into the Yukon Cataclastic Terrane, Yukon Crystalline Terrane and Whitehorse Trough. The Whitehorse Trough lies to the east of the Hoochekoo Fault, west of the Golden Horseshoe project. The Whitehorse Trough comprises Upper Triassic intermediate to basic volcanic capped by carbonate reefs (Povoas Formation) and Lower Jurassic greywacke, shale and conglomerate, derived from the underlying Upper Triassic granitic rocks (Laberge Group). The Yukon Cataclastic Terrane includes hornblende-biotite-chlorite gneiss with interfoliated biotite granite gneiss, Permian Selwyn Gneiss. These units are intruded by younger intrusives and generally show indications of younger structures related to transverse movement along the Tintina Trench. Underlying the Golden Horseshoe project is the early Jurassic McGregor Pluton (Figure 2).

Property Geology

Several notable early surveyors and geologists from the Geological Survey of Canada including Dawson, Ogilvie, and McConnell travelled and are recorded to have inspected several nearby occurrences. H.S. Bostock in a 1936 memoir explicitly detail the geology of the area:

"An area of granitic rocks lies south of Tatlmain lake and between it and Lewes river. It extends only a few miles east of the district where the contact with rocks of the Yukon group runs north and south. This area is apparently composed of granite, quartz monzonite, aplite, pegmatite, quartz porphyry, and partly assimilated bodies of recrystallized older rocks. The southern and eastern parts of the area are mainly occupied by a coarse, grey granite which commonly is porphyritic. The typical rock is slightly gneissoid and a few scattered phenocrysts are present. The phenocrysts vary greatly in abundance, making up much of the rock in some localities and being lacking in others. They are composed of orthoclase and microcline. In the groundmass, quartz is the chief constituent. Orthoclase and oligoclase are both abundant and some microcline is also present. Hornblende and biotite occur in variable quantities. Muscovite, apatite, titanite, magnetite, and epidote are present. In composition, the rock is a granite, but approaches quartz monzonite. In the northern parts of the area and over considerable areas in the central part the rock is light grey or white, medium to moderately fine grained, and commonly slightly foliated. Under the microscope quartz is seen to be the main constituent. Acid oligoclase, orthoclase, microcline, biotite, and hornblende are essential constituents, and muscovite, epidote, titanite, and magnetite are accessory. The rock is a quartz monzonite. It forms sheets in the granite and appears to intrude it, though this is not altogether certain. Both the granite and quartz monzonite are cut by narrow pegmatite and aplite dykes in many places and in one place a fine-grained quartz porphyry cuts the granite. The granite and the quartz monzonite contain areas of hornblende gneiss thought to be roof pendants of the Yukon group. They intrude the Mount Nansen group and in places near the contact the volcanics are recrystallized and schistose."

In 2002 the area was in part combined with the Yukon Targeted Geoscience Initiative, accelerated bedrock mapping and till geochemistry for the Glenlyon (105L/1-7, 11-14) and northeast Carmacks (115I/9,16) areas, central Yukon. An exert from the report describes the underlying McGregor pluton:

"The Tatchun and McGregor batholiths are both composed of three intrusive phases. The earliest phase is a variably foliated, coarse -grained equigranular hornblende -biotite granodiorite. It is locally hornblende porphyritic. Rare gabbro is also associated with this phase of the Early Jurassic plutons. Biotite gabbro appears to be the earliest phase at the north end of Tatchun Batholith (105L/5; Colpron et al., 2002). A small body of augite gabbro to pyroxenite also occurs in the northernMcGregor Batholith (115I/9). The granodiorite phase is intruded by medium-grained K-feldspar megacrystic granodiorite. The megacrystic phase is locally weakly foliated. Both phases of granodiorite typically contain magmatic

epidote indicating a minimum crystallization pressure of 6 kbar (Zen and Hammarstrom, 1984; Zen, 1989). The youngest phase is a beige -weathering, unfoliated, fine -grained leucogranite and aplite."

No historic exploration work is recorded in the GHP area and immediate vicinity; however, based on underlying geology, regional geophysics, and nearby mineralization the exploration target is porphyry and intrusion-related styles of mineralization. The property is positioned within 50 km radius to one producing mines and multiple proven porphyry deposits. The project area lies approximately 50km southeast of the operating Minto Mine a deformed alkaline Cu-Au porphyry with a sulphide resource of 70.8 Mt grading 1.2 % Cu, 0.5 g.t Au and 4.2 g/t Ag (Mercer and Sagman, 2012). Approximately 50 Km to the southwest is the Freegold Mountain area, porphyry and intrusion-related deposits include; Tinta Hill (intrusion related vein), Revenue (Cu, Au, Mo porphyry), La Forma (high-sulphidation epithermal), and Guder (Au skarn). The closest significant mineralization is 30 km to the southwest the Copper North porphyry supergene deposit with an indicated and measured resource of 15.69 million tonnes oxide ore grading 0.94% Cu and 0.38g/t Au as of 2016.

Results and Expenditures

See attached geophysical report provided by Precision Geophysics

Geophysical Survey	$45,000.00

Conclusion and Recommendations

The Golden Horseshoe property is situated in the Tintina Gold Belt, a zone of gold mineralization between the Tintina and Denali faults. The property is positioned within 50 km radius to one producing mines and multiple proven porphyry deposits. The project area lies approximately 50km southeast of the operating Minto Mine a deformed alkaline Cu-Au porphyry with a sulphide resource of 70.8 Mt grading 1.2 % Cu, 0.5 g.t Au and 4.2 g/t Ag (Mercer and Sagman, 2012). Approximately 50 Km to the southwest is the Freegold Mountain area, porphyry and intrusion-related deposits include; Tinta Hill (intrusion related vein), Revenue (Cu, Au, Mo porphyry), La Forma (high-sulphidation epithermal), and Guder (Au skarn). The closest significant mineralization is 30 km to the southwest the Copper North porphyry supergene deposit with an indicated and measured resource of 15.69 million tonnes oxide ore grading 0.94% Cu and 0.38g/t Au as of 2016.

The McGregor Pluton is on the front line of this extensively active area of porphyry and intrusion-related mineralization, yet the area is virgin to exploration. The 9km x 14km anomaly could hold potential for a large-scale bulk tonnage porphyry deposit.

The geological setting of a younger intrusive intruding another older intrusive is analogous to the Casino deposit located 130 km to the northwest. At Casino, the primary supergene enrichment occurs beneath the leech cap at approximately 300m depth.

Further work is recommended to determine if there is an underlying porphyry potential based on the promising results form the 2018 airborne geophysical survey. The survey provides a clear magnetic anomaly typical of a intrusive contact or ring dyke complex that are associated with porphyry style mineralization. The radiometric data highlights zones of alteration. Recommended work consisting of a preliminary soil geochemical survey should be carried out in preparation for future drilling.

Statement of Qualifications

I Nicolai Goeppel am a local Yukon prospector/geologist and owner to Higher Ground Exploration Services. I completed a BSc Earth Sciences program at Memorial University in 2014. I'm born and raised in the Yukon with placer roots in the Freegold Mountain area near Carmacks. I've been involved in geology since 2009 starting with two field seasons with the YGS and have since worked in the mineral exploration industry all across Yukon, BC and in parts of Newfoundland. This work entailed prospecting, bedrock mapping, soil/silt/biochemical sampling, ground VLF/magnetics/EM surveys. This experience also involved management and planning of numerous green field exploration projects. More recently in 2016 and 2017 where I managed and planned a multi-million-dollar exploration program that encompassed the BC coastal mountains from Bute inlet to Atlin, BC that ground truthed over 300 targets and personally discovered multiple high grade finds including grades up to 36,875 g/t Ag and 92.8 g/t Au from brand new hardrock discoveries. The discoveries led to property options to both Goliath resources and Juggernaut exploration. In addition, I visited various world class porphyry and related deposits in Chile and Bolivia, including Chuquicamata, Cerro Rico and Escondida.

Reference

Bond, J.D. and Plouffe, A., 2003. Yukon Targeted Geoscience Initiative, Part 2: Glacial history, till geochemistry and new mineral exploration targets in Glenlyon and eastern Carmacks map area, central Yukon. In: Yukon Exploration and Geology 2002, D.S. Emond and L.L. Lewis (eds.), Exploration and Geological Services Division, Yukon Region, Indian and Northern Affairs Canada, p. 109 -134.

Bostock, Hugh Samuel. Mining Industry of Yukon, 1935. JO Patenaude, 1936.

Colpron, M., et al. "Yukon Targeted Geoscience Initiative: Part 1. Results of accelerated bedrock mapping in Glenlyon (105L/1-7, 11-14) and northeast Carmacks (115I/9, 16) areas, central Yukon." Yukon exploration and geology (2002): 85-108.

Copland, H., 1987: "Geological and Geochemical Report on the Main Claims": Yukon Energy, Mines and Resources, Assessment Report No 091954.

Holliday, J. R., and D. R. Cooke. "Advances in geological models and exploration methods for copper±gold porphyry deposits." Proceedings of exploration. Vol. 7. 2007.

Mercer, B. and Sagman, J., 2012 Phase VI Preliminary Feasibility Report Minto Mine. Internal report, Minto Explorations Ltd., 368 p.

Rowe, R. R., and X. Zhou. "Models and exploration methods for major gold deposit types." Proceedings of Exploration. Vol. 7. 2007.

Rowins, Stephen M. "Reduced porphyry copper-gold deposits: A new variation on an old theme." Geology 28.6 (2000): 491-494.

Appendix I

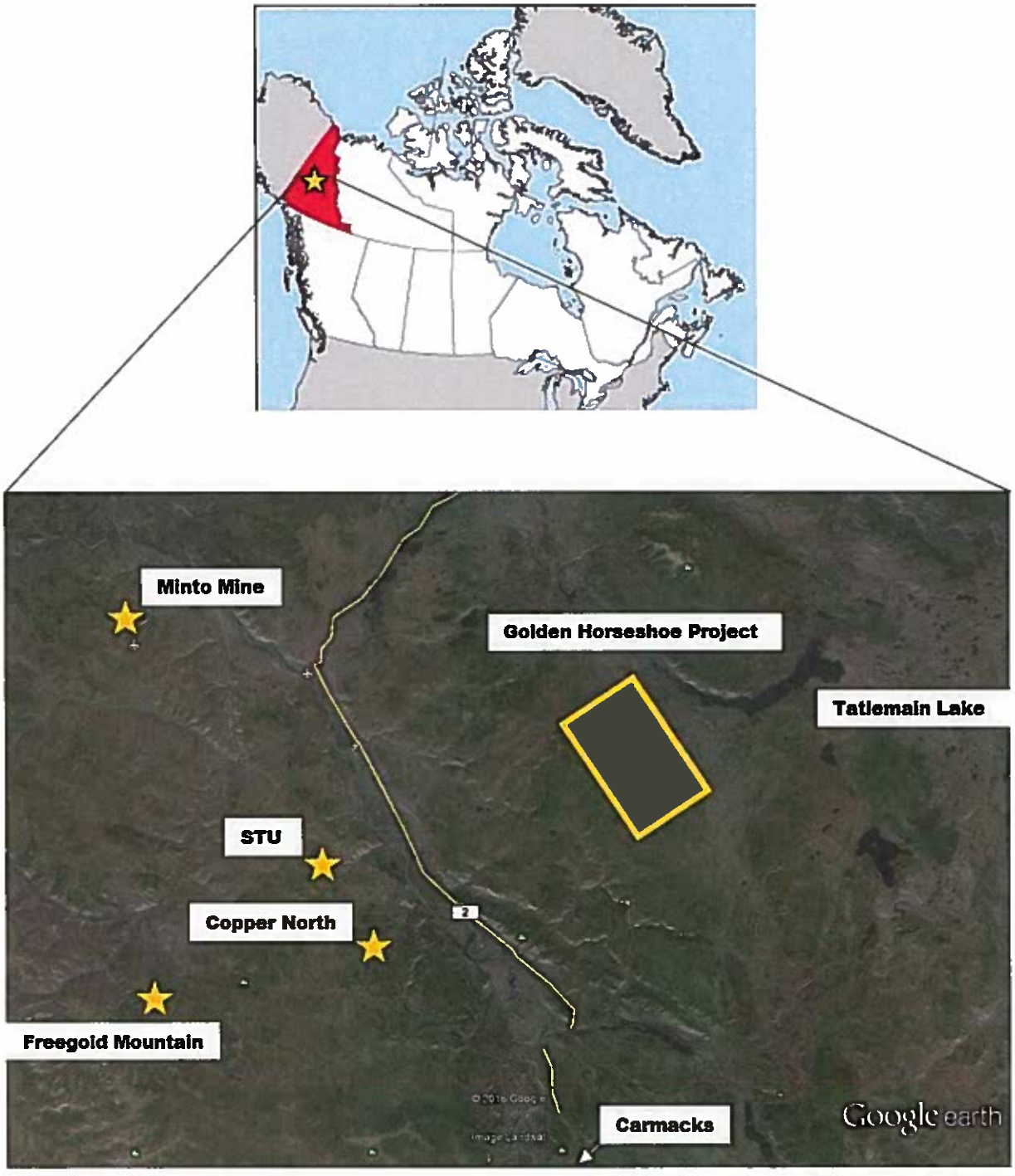

Figure 1. Location

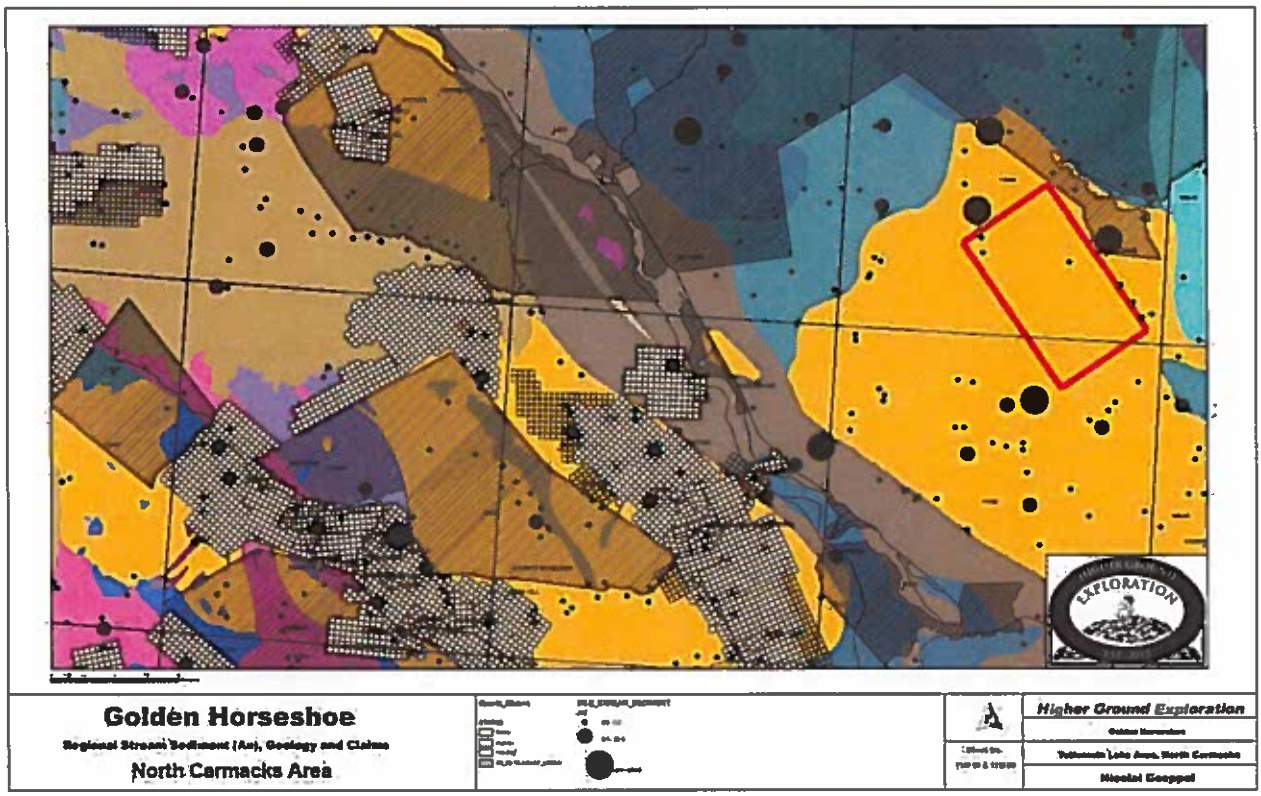

Figure 2. Geology and Au-in-silt RGS.

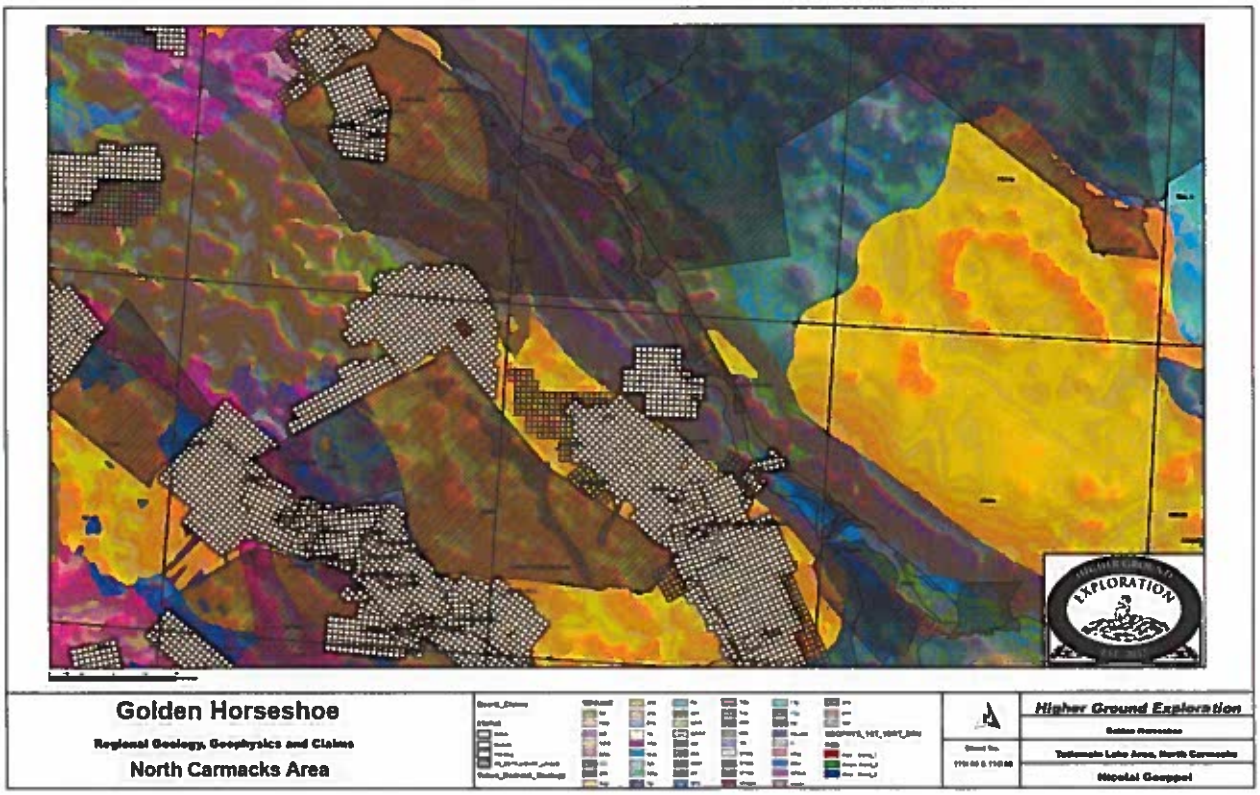

Figure 3. Geology over regional First Vertical Derivative.

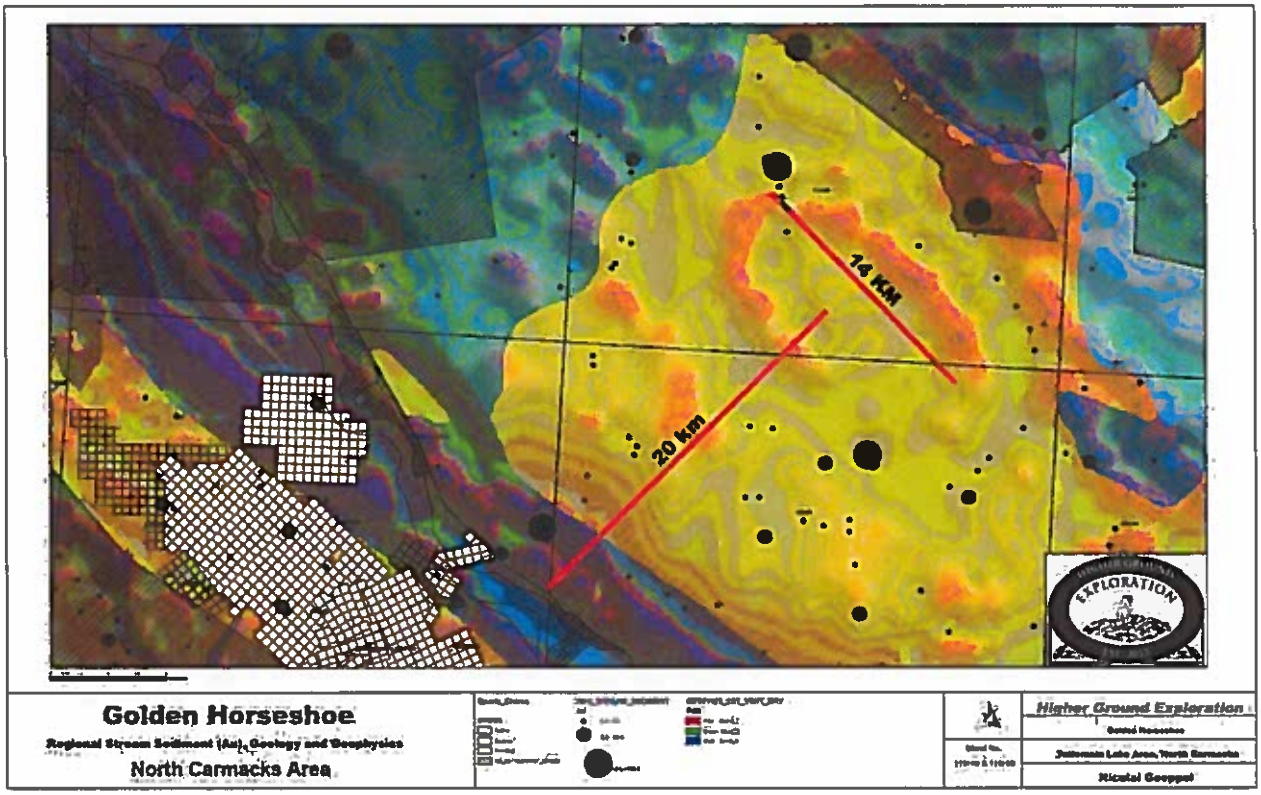

Figure 4. Close up on Horseshoe anomaly.

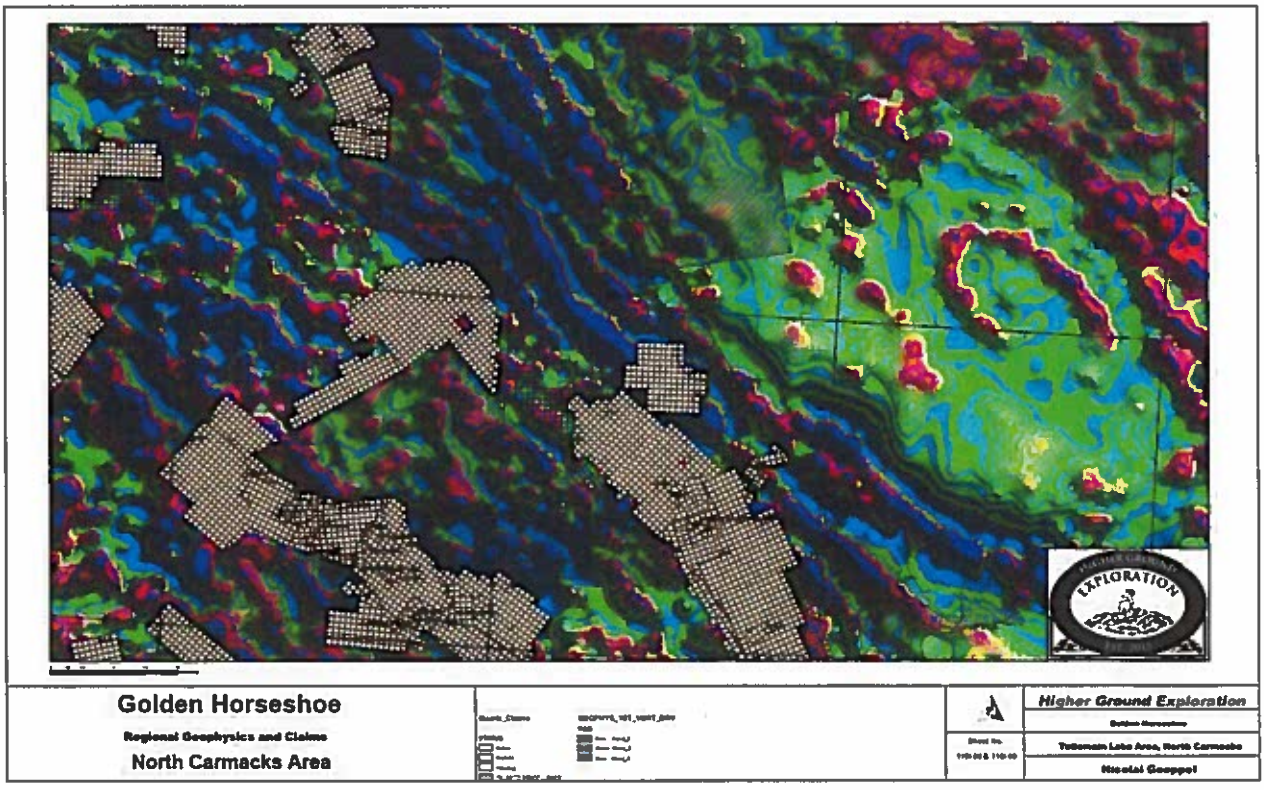

Figure 5. Regional First Vertical Derivative.

Figure 6. Regional Geology.

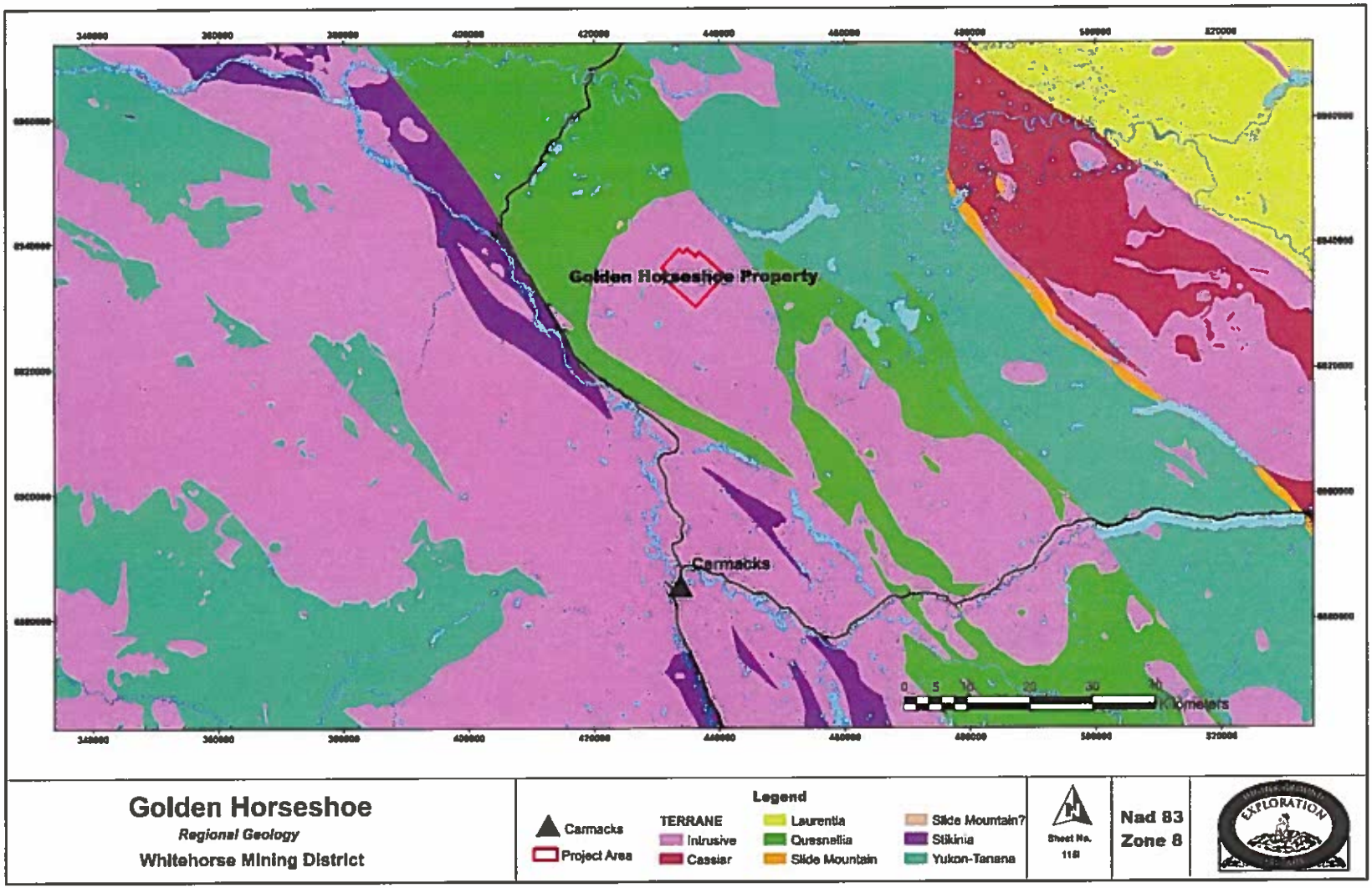

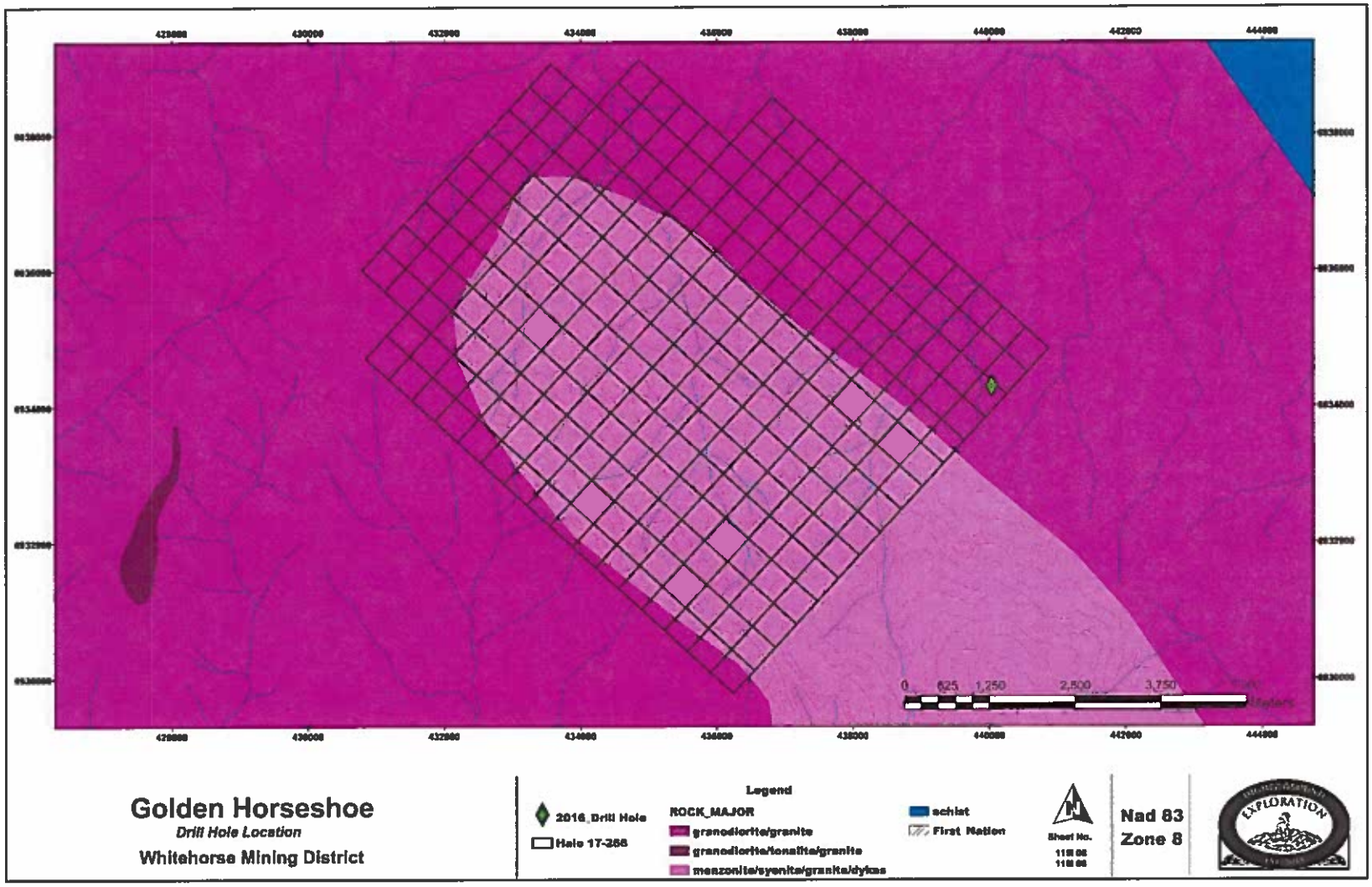

Figure 7. 2016 Drill Hole Location.

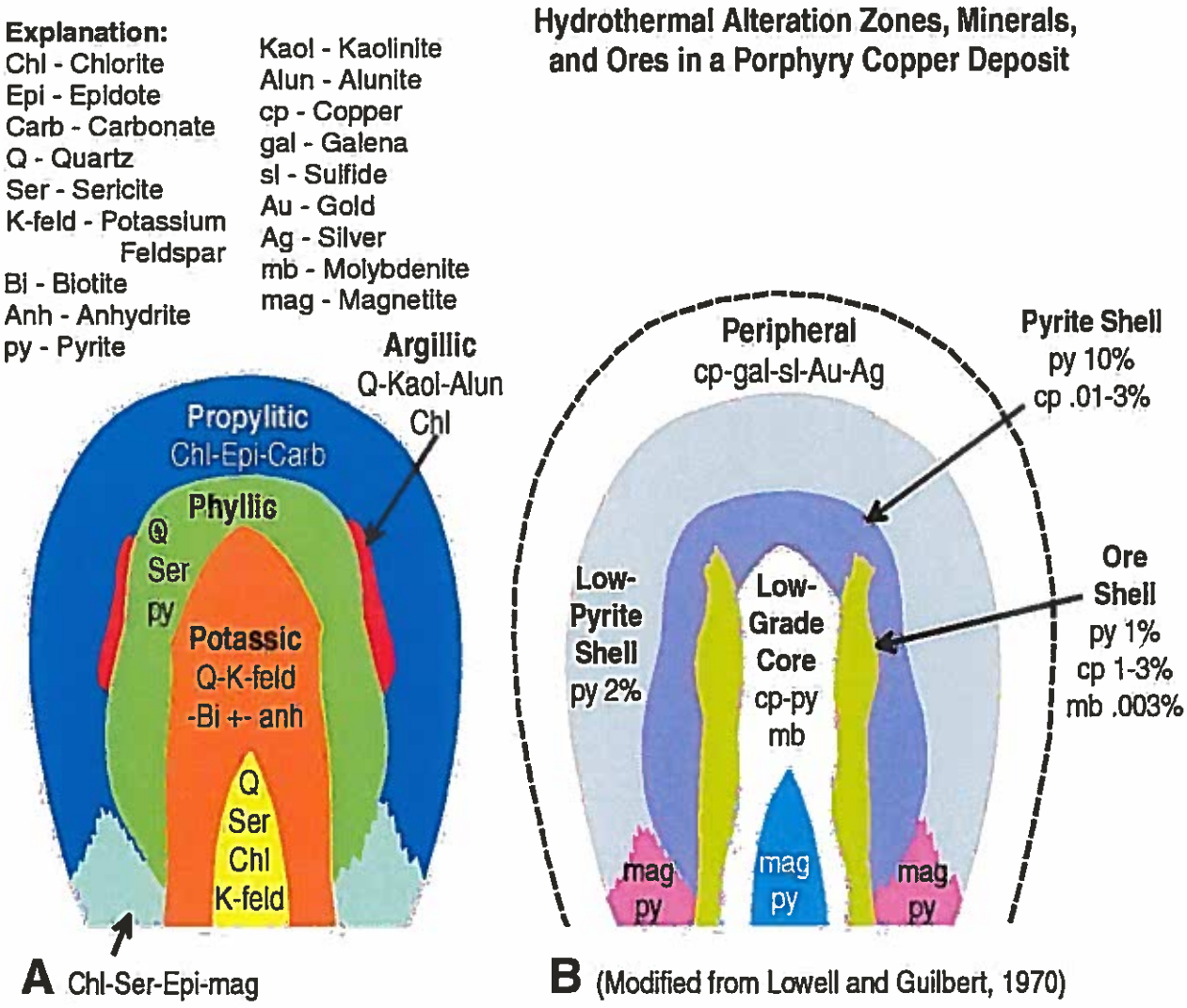

Figure 8. Modified Lowell and Guilbert outlining general zonations in a porphyry system.

Grant Number	Claim Name	Claim Nbr	Claim Owner	Claim Expiry Date	Status
YF50057	HALO	17	Thi My Linh Pham - 100%	2018-08-16	Active
YF50058	HALO	18	Thi My Linh Pham - 100%	2018-08-16	Active
YF50059	HALO	19	Thi My Linh Pham - 100%	2018-08-16	Active
YF50060	HALO	20	Thi My Linh Pham - 100%	2018-08-16	Active
YF50061	HALO	21	Thi My Linh Pham - 100%	2018-08-16	Active
YF50062	HALO	22	Thi My Linh Pham - 100%	2018-08-16	Active
YF50063	HALO	23	Thi My Linh Pham - 100%	2018-08-16	Active
YF50064	HALO	24	Thi My Linh Pham - 100%	2018-08-16	Active
YF50065	HALO	25	Thi My Linh Pham - 100%	2018-08-16	Active
YF50066	HALO	26	Thi My Linh Pham - 100%	2018-08-16	Active
YF50067	HALO	27	Thi My Linh Pham - 100%	2018-08-16	Active
YF50068	HALO	28	Thi My Linh Pham - 100%	2018-08-16	Active
YF50069	HALO	29	Thi My Linh Pham - 100%	2018-08-16	Active
YF50070	HALO	30	Thi My Linh Pham - 100%	2018-08-16	Active
YF50071	HALO	31	Thi My Linh Pham - 100%	2018-08-16	Active
YF50072	HALO	32	Thi My Linh Pham - 100%	2018-08-16	Active
YF50073	HALO	33	Thi My Linh Pham - 100%	2018-08-16	Active
YF50074	HALO	34	Thi My Linh Pham - 100%	2018-08-16	Active
YF50075	HALO	35	Thi My Linh Pham - 100%	2018-08-16	Active
YF50076	HALO	36	Thi My Linh Pham - 100%	2018-08-16	Active
YF50077	HALO	37	Thi My Linh Pham - 100%	2018-08-16	Active
YF50078	HALO	38	Thi My Linh Pham - 100%	2018-08-16	Active
YF50079	HALO	39	Thi My Linh Pham - 100%	2018-08-16	Active
YF50080	HALO	40	Thi My Linh Pham - 100%	2018-08-16	Active
YF50081	HALO	41	Thi My Linh Pham - 100%	2018-08-16	Active
YF50082	HALO	42	Thi My Linh Pham - 100%	2018-08-16	Active
YF50083	HALO	43	Thi My Linh Pham - 100%	2018-08-16	Active
YF50084	HALO	44	Thi My Linh Pham - 100%	2018-08-16	Active
YF50085	HALO	45	Thi My Linh Pham - 100%	2018-08-16	Active
YF50086	HALO	46	Thi My Linh Pham - 100%	2018-08-16	Active
YF50087	HALO	47	Thi My Linh Pham - 100%	2018-08-16	Active
YF50088	HALO	48	Thi My Linh Pham - 100%	2018-08-16	Active
YF50089	HALO	49	Thi My Linh Pham - 100%	2018-08-16	Active
YF50090	HALO	50	Thi My Linh Pham - 100%	2018-08-16	Active
YF50091	HALO	51	Thi My Linh Pham - 100%	2018-08-16	Active
YF50092	HALO	52	Thi My Linh Pham - 100%	2018-08-16	Active
YF50093	HALO	53	Thi My Linh Pham - 100%	2018-08-16	Active
YF50094	HALO	54	Thi My Linh Pham - 100%	2018-08-16	Active
YF50095	HALO	55	Thi My Linh Pham - 100%	2018-08-16	Active
YF50096	HALO	56	Thi My Linh Pham - 100%	2018-08-16	Active
YF50097	HALO	57	Thi My Linh Pham - 100%	2018-08-16	Active

YF50098	HALO	58	Thi My Linh Pham - 100%	2018-08-16	Active
YF50099	HALO	59	Thi My Linh Pham - 100%	2018-08-16	Active
YF50100	HALO	60	Thi My Linh Pham - 100%	2018-08-16	Active
YF50415	HALO	61	Thi My Linh Pham - 100%	2018-08-16	Active
YF50416	HALO	62	Thi My Linh Pham - 100%	2018-08-16	Active
YF50417	HALO	63	Thi My Linh Pham - 100%	2018-08-16	Active
YF50418	HALO	64	Thi My Linh Pham - 100%	2018-08-16	Active
YF50419	HALO	65	Thi My Linh Pham - 100%	2018-08-16	Active
YF50420	HALO	66	Thi My Linh Pham - 100%	2018-08-16	Active
YF50421	HALO	67	Thi My Linh Pham - 100%	2018-08-16	Active
YF50422	HALO	68	Thi My Linh Pham - 100%	2018-08-16	Active
YF50423	HALO	69	Thi My Linh Pham - 100%	2018-08-16	Active
YF50424	HALO	70	Thi My Linh Pham - 100%	2018-08-16	Active
YF50425	HALO	71	Thi My Linh Pham - 100%	2018-08-16	Active
YF50426	HALO	72	Thi My Linh Pham - 100%	2018-08-16	Active
YF50427	HALO	73	Thi My Linh Pham - 100%	2018-08-16	Active
YF50428	HALO	74	Thi My Linh Pham - 100%	2018-08-16	Active
YF50429	HALO	75	Thi My Linh Pham - 100%	2018-08-16	Active
YF50430	HALO	76	Thi My Linh Pham - 100%	2018-08-16	Active
YF50431	HALO	77	Thi My Linh Pham - 100%	2018-08-16	Active
YF50432	HALO	78	Thi My Linh Pham - 100%	2018-08-16	Active
YF50433	HALO	79	Thi My Linh Pham - 100%	2018-08-16	Active
YF50434	HALO	80	Thi My Linh Pham - 100%	2018-08-16	Active
YF50435	HALO	81	Thi My Linh Pham - 100%	2018-08-16	Active
YF50436	HALO	82	Thi My Linh Pham - 100%	2018-08-16	Active
YF50437	HALO	83	Thi My Linh Pham - 100%	2018-08-16	Active
YF50438	HALO	84	Thi My Linh Pham - 100%	2018-08-16	Active
YF50439	HALO	85	Thi My Linh Pham - 100%	2018-08-16	Active
YF50440	HALO	86	Thi My Linh Pham - 100%	2018-08-16	Active
YF50441	HALO	87	Thi My Linh Pham - 100%	2018-08-16	Active
YF50442	HALO	88	Thi My Linh Pham - 100%	2018-08-16	Active
YF50443	HALO	89	Thi My Linh Pham - 100%	2018-08-16	Active
YF50444	HALO	90	Thi My Linh Pham - 100%	2018-08-16	Active
YF50445	HALO	91	Thi My Linh Pham - 100%	2018-08-16	Active
YF50446	HALO	92	Thi My Linh Pham - 100%	2018-08-16	Active
YF50447	HALO	93	Thi My Linh Pham - 100%	2018-08-16	Active
YF50448	HALO	94	Thi My Linh Pham - 100%	2018-08-16	Active
YF50449	HALO	95	Thi My Linh Pham - 100%	2018-08-16	Active
YF50450	HALO	96	Thi My Linh Pham - 100%	2018-08-16	Active
YF50451	HALO	97	Thi My Linh Pham - 100%	2018-08-16	Active
YF50452	HALO	98	Thi My Linh Pham - 100%	2018-08-16	Active
YF50453	HALO	99	Thi My Linh Pham - 100%	2018-08-16	Active
YF50454	HALO	100	Thi My Linh Pham - 100%	2018-08-16	Active

YF50455	HALO	101	Thi My Linh Pham - 100%	2018-08-16	Active
YF50456	HALO	102	Thi My Linh Pham - 100%	2018-08-16	Active
YF50457	HALO	103	Thi My Linh Pham - 100%	2018-08-16	Active
YF50458	HALO	104	Thi My Linh Pham - 100%	2018-08-16	Active
YF50459	HALO	105	Thi My Linh Pham - 100%	2018-08-16	Active
YF50460	HALO	106	Thi My Linh Pham - 100%	2018-08-16	Active
YF50461	HALO	107	Thi My Linh Pham - 100%	2018-08-16	Active
YF50462	HALO	108	Thi My Linh Pham - 100%	2018-08-16	Active
YF50463	HALO	109	Thi My Linh Pham - 100%	2018-08-16	Active
YF50464	HALO	110	Thi My Linh Pham - 100%	2018-08-16	Active
YF50465	HALO	111	Thi My Linh Pham - 100%	2018-08-16	Active
YF50466	HALO	112	Thi My Linh Pham - 100%	2018-08-16	Active
YF50467	HALO	113	Thi My Linh Pham - 100%	2018-08-16	Active
YF50468	HALO	114	Thi My Linh Pham - 100%	2018-08-16	Active
YF50469	HALO	115	Thi My Linh Pham - 100%	2018-08-16	Active
YF50470	HALO	116	Thi My Linh Pham - 100%	2018-08-16	Active
YF50471	HALO	117	Thi My Linh Pham - 100%	2018-08-16	Active
YF50472	HALO	118	Thi My Linh Pham - 100%	2018-08-16	Active
YF50473	HALO	119	Thi My Linh Pham - 100%	2018-08-16	Active
YF50474	HALO	120	Thi My Linh Pham - 100%	2018-08-16	Active
YF50475	HALO	121	Thi My Linh Pham - 100%	2018-08-16	Active
YF50476	HALO	122	Thi My Linh Pham - 100%	2018-08-16	Active
YF50477	HALO	123	Thi My Linh Pham - 100%	2018-08-16	Active
YF50478	HALO	124	Thi My Linh Pham - 100%	2018-08-16	Active
YF50479	HALO	125	Thi My Linh Pham - 100%	2018-08-16	Active
YF50480	HALO	126	Thi My Linh Pham - 100%	2018-08-16	Active
YF50481	HALO	127	Thi My Linh Pham - 100%	2018-08-16	Active
YF50482	HALO	128	Thi My Linh Pham - 100%	2018-08-16	Active
YF50483	HALO	129	Thi My Linh Pham - 100%	2018-08-16	Active
YF50484	HALO	130	Thi My Linh Pham - 100%	2018-08-16	Active
YF50485	HALO	131	Thi My Linh Pham - 100%	2018-08-16	Active
YF50486	HALO	132	Thi My Linh Pham - 100%	2018-08-16	Active
YF50487	HALO	133	Thi My Linh Pham - 100%	2018-08-16	Active
YF50488	HALO	134	Thi My Linh Pham - 100%	2018-08-16	Active
YF50489	HALO	135	Thi My Linh Pham - 100%	2018-08-16	Active
YF50490	HALO	136	Thi My Linh Pham - 100%	2018-08-16	Active
YF50491	HALO	137	Thi My Linh Pham - 100%	2018-08-16	Active
YF50492	HALO	138	Thi My Linh Pham - 100%	2018-08-16	Active
YF50493	HALO	139	Thi My Linh Pham - 100%	2018-08-16	Active
YF50494	HALO	140	Thi My Linh Pham - 100%	2018-08-16	Active
YF50495	HALO	141	Thi My Linh Pham - 100%	2018-08-16	Active
YF50496	HALO	142	Thi My Linh Pham - 100%	2018-08-16	Active
YF50497	HALO	143	Thi My Linh Pham - 100%	2018-08-16	Active

YF50498	HALO	144	Thi My Linh Pham - 100%	2018-08-16	Active
YF50499	HALO	145	Thi My Linh Pham - 100%	2018-08-16	Active
YF50500	HALO	146	Thi My Linh Pham - 100%	2018-08-16	Active
YF50501	HALO	147	Thi My Linh Pham - 100%	2018-08-16	Active
YF50502	HALO	148	Thi My Linh Pham - 100%	2018-08-16	Active
YF50503	HALO	149	Thi My Linh Pham - 100%	2018-08-16	Active
YF50504	HALO	150	Thi My Linh Pham - 100%	2018-08-16	Active
YF50505	HALO	151	Thi My Linh Pham - 100%	2018-08-16	Active
YF50506	HALO	152	Thi My Linh Pham - 100%	2018-08-16	Active
YF50507	HALO	153	Thi My Linh Pham - 100%	2018-08-16	Active
YF50508	HALO	154	Thi My Linh Pham - 100%	2018-08-16	Active
YF50509	HALO	155	Thi My Linh Pham - 100%	2018-08-16	Active
YF50510	HALO	156	Thi My Linh Pham - 100%	2018-08-16	Active
YF50511	HALO	157	Thi My Linh Pham - 100%	2018-08-16	Active
YF50512	HALO	158	Thi My Linh Pham - 100%	2018-08-16	Active
YF50513	HALO	159	Thi My Linh Pham - 100%	2018-08-16	Active
YF50514	HALO	160	Thi My Linh Pham - 100%	2018-08-16	Active
YF50515	HALO	161	Thi My Linh Pham - 100%	2018-08-16	Active
YF50516	HALO	162	Thi My Linh Pham - 100%	2018-08-16	Active
YF50517	HALO	163	Thi My Linh Pham - 100%	2018-08-16	Active
YF50518	HALO	164	Thi My Linh Pham - 100%	2018-08-16	Active
YF50519	HALO	165	Thi My Linh Pham - 100%	2018-08-16	Active
YF50520	HALO	166	Thi My Linh Pham - 100%	2018-08-16	Active
YF50521	HALO	167	Thi My Linh Pham - 100%	2018-08-16	Active
YF50522	HALO	168	Thi My Linh Pham - 100%	2018-08-16	Active
YF50523	HALO	169	Thi My Linh Pham - 100%	2018-08-16	Active
YF50524	HALO	170	Thi My Linh Pham - 100%	2018-08-16	Active
YF50525	HALO	171	Thi My Linh Pham - 100%	2018-08-16	Active
YF50526	HALO	172	Thi My Linh Pham - 100%	2018-08-16	Active
YF50527	HALO	173	Thi My Linh Pham - 100%	2018-08-16	Active
YF50528	HALO	174	Thi My Linh Pham - 100%	2018-08-16	Active
YF50529	HALO	175	Thi My Linh Pham - 100%	2018-08-16	Active
YF50530	HALO	176	Thi My Linh Pham - 100%	2018-08-16	Active
YF50531	HALO	177	Thi My Linh Pham - 100%	2018-08-16	Active
YF50532	HALO	178	Thi My Linh Pham - 100%	2018-08-16	Active
YF50533	HALO	179	Thi My Linh Pham - 100%	2018-08-16	Active
YF50534	HALO	180	Thi My Linh Pham - 100%	2018-08-16	Active
YF50535	HALO	181	Thi My Linh Pham - 100%	2018-08-16	Active
YF50536	HALO	182	Thi My Linh Pham - 100%	2018-08-16	Active
YF50537	HALO	183	Thi My Linh Pham - 100%	2018-08-16	Active
YF50538	HALO	184	Thi My Linh Pham - 100%	2018-08-16	Active
YF50539	HALO	185	Thi My Linh Pham - 100%	2018-08-16	Active
YF50540	HALO	186	Thi My Linh Pham - 100%	2018-08-16	Active

YF50541	HALO	187	Thi My Linh Pham - 100%	2018-08-16	Active
YF50542	HALO	188	Thi My Linh Pham - 100%	2018-08-16	Active
YF50543	HALO	189	Thi My Linh Pham - 100%	2018-08-16	Active
YF50544	HALO	190	Thi My Linh Pham - 100%	2018-08-16	Active
YF50545	HALO	191	Thi My Linh Pham - 100%	2018-08-16	Active
YF50546	HALO	192	Thi My Linh Pham - 100%	2018-08-16	Active
YF50547	HALO	193	Thi My Linh Pham - 100%	2018-08-16	Active
YF50548	HALO	194	Thi My Linh Pham - 100%	2018-08-16	Active
YF50549	HALO	195	Thi My Linh Pham - 100%	2018-08-16	Active
YF50550	HALO	196	Thi My Linh Pham - 100%	2018-08-16	Active
YF50551	HALO	197	Thi My Linh Pham - 100%	2018-08-16	Active
YF50552	HALO	198	Thi My Linh Pham - 100%	2018-08-16	Active
YF50553	HALO	199	Thi My Linh Pham - 100%	2018-08-16	Active
YF50554	HALO	200	Thi My Linh Pham - 100%	2018-08-16	Active
YF50555	HALO	201	Thi My Linh Pham - 100%	2018-08-16	Active
YF50556	HALO	202	Thi My Linh Pham - 100%	2018-08-16	Active
YF50557	HALO	203	Thi My Linh Pham - 100%	2018-08-16	Active
YF50558	HALO	204	Thi My Linh Pham - 100%	2018-08-16	Active
YF50559	HALO	205	Thi My Linh Pham - 100%	2018-08-16	Active
YF50560	HALO	206	Thi My Linh Pham - 100%	2018-08-16	Active
YF50561	HALO	207	Thi My Linh Pham - 100%	2018-08-16	Active
YF50562	HALO	208	Thi My Linh Pham - 100%	2018-08-16	Active
YF50563	HALO	209	Thi My Linh Pham - 100%	2018-08-16	Active
YF50564	HALO	210	Thi My Linh Pham - 100%	2018-08-16	Active
YF52021	HALO	211	Thi My Linh Pham - 100%	2018-08-16	Active
YF52022	HALO	212	Thi My Linh Pham - 100%	2018-08-16	Active
YF52023	HALO	213	Thi My Linh Pham - 100%	2018-08-16	Active
YF52024	HALO	214	Thi My Linh Pham - 100%	2018-08-16	Active
YF52025	HALO	215	Thi My Linh Pham - 100%	2018-08-16	Active
YF52026	HALO	216	Thi My Linh Pham - 100%	2018-08-16	Active
YF52027	HALO	217	Thi My Linh Pham - 100%	2018-08-16	Active
YF52028	HALO	218	Thi My Linh Pham - 100%	2018-08-16	Active
YF52029	HALO	219	Thi My Linh Pham - 100%	2018-08-16	Active
YF52030	HALO	220	Thi My Linh Pham - 100%	2018-08-16	Active
YF52031	HALO	221	Thi My Linh Pham - 100%	2018-08-16	Active
YF52032	HALO	222	Thi My Linh Pham - 100%	2018-08-16	Active
YF52033	HALO	223	Thi My Linh Pham - 100%	2018-08-16	Active
YF52034	HALO	224	Thi My Linh Pham - 100%	2018-08-16	Active
YF52035	HALO	225	Thi My Linh Pham - 100%	2018-08-16	Active
YF52036	HALO	226	Thi My Linh Pham - 100%	2018-08-16	Active
YF52037	HALO	227	Thi My Linh Pham - 100%	2018-08-16	Active
YF52038	HALO	228	Thi My Linh Pham - 100%	2018-08-16	Active
YF52039	HALO	229	Thi My Linh Pham - 100%	2018-08-16	Active

YF52040	HALO	230	Thi My Linh Pham - 100%	2018-08-16	Active
YF52041	HALO	231	Thi My Linh Pham - 100%	2018-08-16	Active
YF52042	HALO	232	Thi My Linh Pham - 100%	2018-08-16	Active
YF52043	HALO	233	Thi My Linh Pham - 100%	2018-08-16	Active
YF52044	HALO	234	Thi My Linh Pham - 100%	2018-08-16	Active
YF52045	HALO	235	Thi My Linh Pham - 100%	2018-08-16	Active
YF52046	HALO	236	Thi My Linh Pham - 100%	2018-08-16	Active
YF52047	HALO	237	Thi My Linh Pham - 100%	2018-08-16	Active
YF52048	HALO	238	Thi My Linh Pham - 100%	2018-08-16	Active
YF52049	HALO	239	Thi My Linh Pham - 100%	2018-08-16	Active
YF52050	HALO	240	Thi My Linh Pham - 100%	2018-08-16	Active
YF52051	HALO	241	Thi My Linh Pham - 100%	2018-08-16	Active
YF52052	HALO	242	Thi My Linh Pham - 100%	2018-08-16	Active
YF52053	HALO	243	Thi My Linh Pham - 100%	2018-08-16	Active
YF52054	HALO	244	Thi My Linh Pham - 100%	2018-08-16	Active
YF52055	HALO	245	Thi My Linh Pham - 100%	2018-08-16	Active
YF52056	HALO	246	Thi My Linh Pham - 100%	2018-08-16	Active
YF52057	HALO	247	Thi My Linh Pham - 100%	2018-08-16	Active
YF52058	HALO	248	Thi My Linh Pham - 100%	2018-08-16	Active
YF52059	HALO	249	Thi My Linh Pham - 100%	2018-08-16	Active
YF52060	HALO	250	Thi My Linh Pham - 100%	2018-08-16	Active
YF52061	HALO	251	Thi My Linh Pham - 100%	2018-08-16	Active
YF52062	HALO	252	Thi My Linh Pham - 100%	2018-08-16	Active
YF52063	HALO	253	Thi My Linh Pham - 100%	2018-08-16	Active
YF52064	HALO	254	Thi My Linh Pham - 100%	2018-08-16	Active
YF52065	HALO	255	Thi My Linh Pham - 100%	2018-08-16	Active
YF52066	HALO	256	Thi My Linh Pham - 100%	2018-08-16	Active
YF52067	HALO	257	Thi My Linh Pham - 100%	2018-08-16	Active
YF52068	HALO	258	Thi My Linh Pham - 100%	2018-08-16	Active
YF52069	HALO	259	Thi My Linh Pham - 100%	2018-08-16	Active
YF52070	HALO	260	Thi My Linh Pham - 100%	2018-08-16	Active
YF52071	HALO	261	Thi My Linh Pham - 100%	2018-08-16	Active
YF52072	HALO	262	Thi My Linh Pham - 100%	2018-08-16	Active
YF52073	HALO	263	Thi My Linh Pham - 100%	2018-08-16	Active
YF52074	HALO	264	Thi My Linh Pham - 100%	2018-08-16	Active
YF52075	HALO	265	Thi My Linh Pham - 100%	2018-08-16	Active
YF52076	HALO	266	Thi My Linh Pham - 100%	2018-08-16	Active

Figure 9. Claim Status

Figure 10. Claim Map

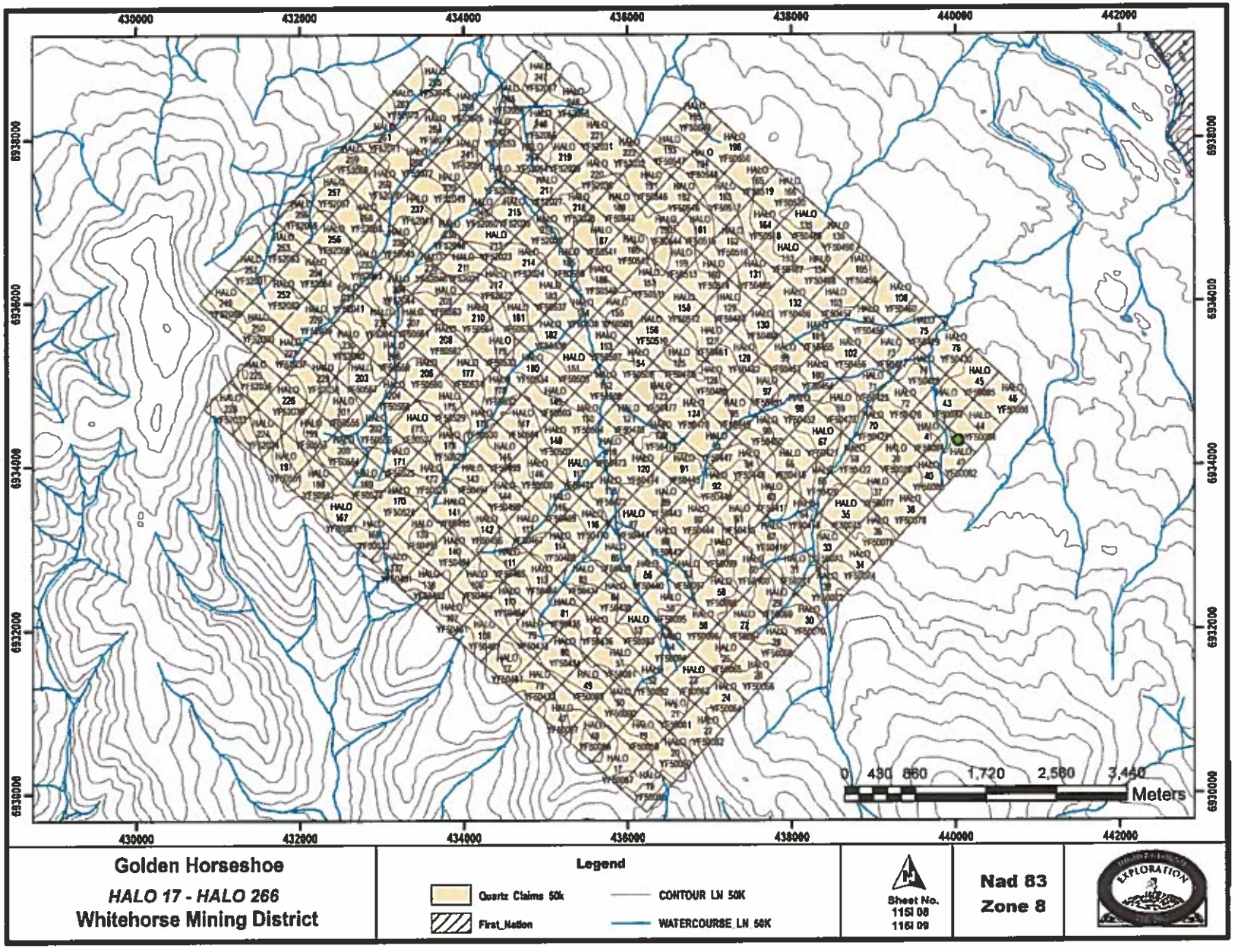

Precision GeoSurveys

AIRBORNE GEOPHYSICAL SURVEY REPORT

Golden Horseshoe Survey Block

Carmacks, Yukon

Kluane Drilling Ltd.

Precision GeoSurveys Inc.
www.precisiongeosurveys.com
Hangar 42 Langley Airport
21330 - 56th Ave., Langley, BC
Canada V2Y 0E5
604-484-9402

Jenny Poon, B.Sc., P.Geo.
Shawn Walker, M.Sc., P.Geo.

July 2018
Job#18106

Table of Contents

List of Figures

List of Tables

List of Appendices

List of Golden Horseshoe Survey Block Plates (in pocket) – Scale 1:25,000

1.0 Introduction

This report outlines the geophysical survey operations and data processing procedures taken during the high resolution helicopter-borne aeromagnetic and radiometric survey flown over Golden Horseshoe survey block located north of Carmacks, Yukon (Figure 1) for Kluane Drilling Ltd. The geophysical survey was started on July 4, 2018 and completed on July 5, 2018.

Figure 1: Golden Horseshoe survey area location map.

1.1 Survey Area

The Golden Horseshoe survey block is centered approximately 50 km north of Carmacks, Yukon (Figure 2).

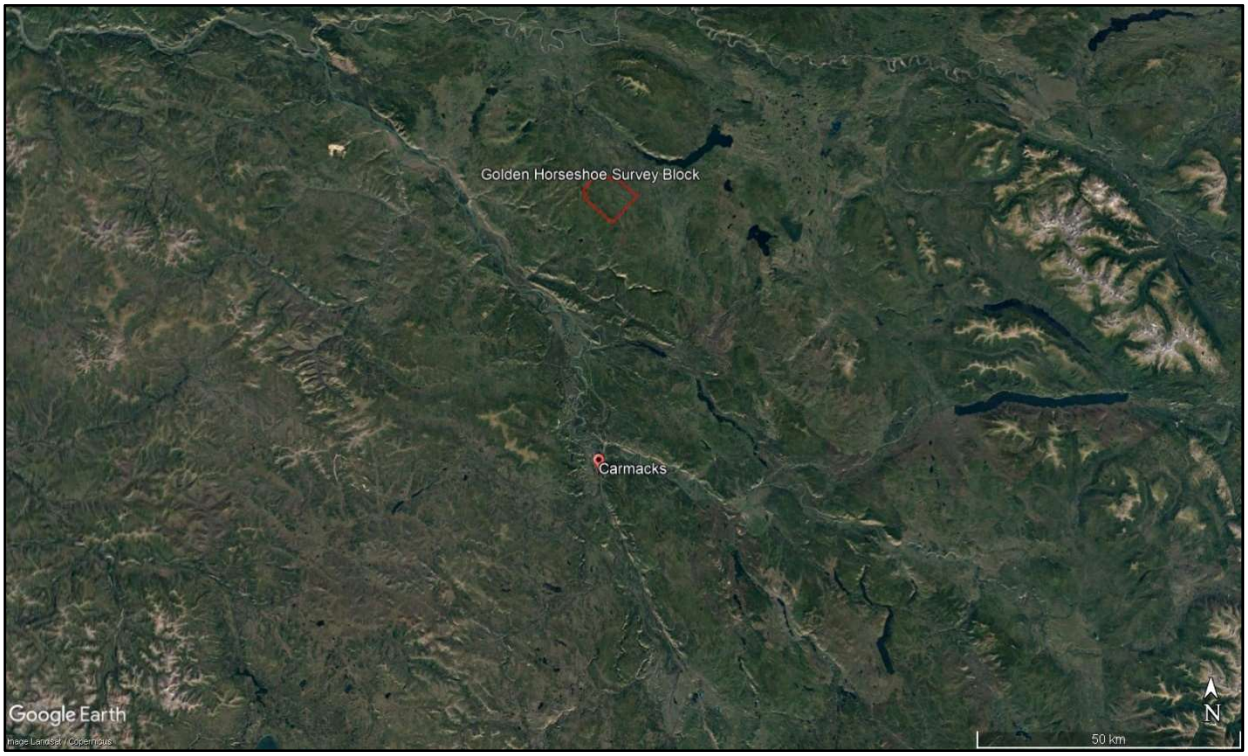

Figure 2: Golden Horseshoe survey block 50 km north of Carmacks, Yukon

A total of 581 line km of magnetic and radiometric data was collected over a total area of 52.5 km^2 (Figures 3 and 4). The survey was flown at 100 meter line spacing at a heading of 043°/223°; tie lines were flown at 1000 meter spacing at a heading of 133°/313°.

Figure 3: Plan View – Golden Horseshoe survey block with actual flight lines displayed in yellow and boundary in red.

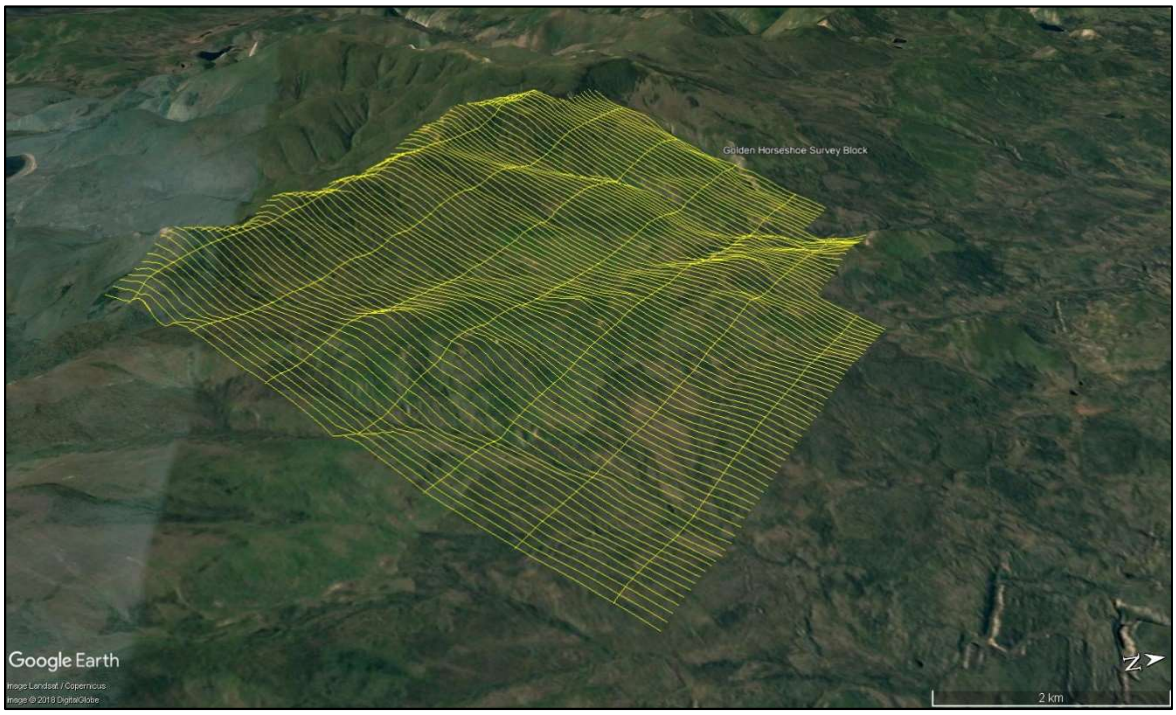

Figure 4: Terrain View – Golden Horseshoe survey block with actual flight lines displayed in yellow.

1.2 Survey Specifications

The geodetic system used for the geophysical survey was WGS 84 in UTM Zone 8N. A total of 581 line km was flown over 52.5 km^2 (Table 1). Polygon coordinates for the survey block are specified in Table 2.

Survey Block	Area (km^2)	Line Type	No. of Lines Planned	No. of Lines Completed	Line Spacing (m)	Line Orientation (UTM grid)	Actual Survey Height (m)	Total Planned Line km	Total Actual km Flown
Golden Horseshoe	52.5	Survey	83	83	100	043°/223°	34.6	528	528
		Tie	7	7	1000	133°/313°	34.6	53	53
		Total	**90**	**90**				**581**	**581**

Table 1: Survey flight line specifications.

Longitude (deg)	Latitude (deg)	Easting (m)	Northing (m)	N/S	E/W
136.34574294	62.54861336	430788	6936020	N	W
136.29304522	62.57640116	433560	6939060	N	W
136.27977281	62.57101123	434230	6938446	N	W
136.26804416	62.57708779	434846	6939111	N	W
136.24118299	62.56633174	436203	6937886	N	W
136.22943141	62.57246807	436820	6938558	N	W
136.14813534	62.53994427	440933	6934858	N	W
136.23739134	62.49378554	436243	6929801	N	W
136.34411255	62.53703936	430845	6934729	N	W
136.33255002	62.54320074	431454	6935403	N	W

Table 2: Golden Horseshoe survey block polygon coordinates using WGS 84 in UTM zone 8N.

2.0 Geophysical Data

Geophysical data are collected in a variety of ways and are used to aid in determination of geology, mineral deposits, oil and gas deposits, geotechnical investigations, contaminated land sites, and UXO (unexploded ordnance) detection.

For the purposes of this survey, airborne magnetic and radiometric data were collected to serve in geological mapping and exploration for mineral deposits.

2.1 Magnetic Data

Magnetic surveying is the most common airborne geophysical technology used for both mineral and hydrocarbon exploration. Aeromagnetic surveys measure and record the total intensity of the magnetic field at the magnetometer sensor, which is a combination of the desired magnetic

field generated in the Earth as well as small variations due to the temporal effects of the constantly varying solar wind and the magnetic field of the survey aircraft. By subtracting the temporal, regional, and aircraft effects, the resulting aeromagnetic map shows the spatial distribution and relative abundance of magnetic minerals - most commonly the iron oxide mineral magnetite - in the upper levels of Earth's crust, which in turn are related to lithology, structure, and alteration of bedrock. Survey specifications, instrumentation, and interpretation procedures depend on the objectives of the survey. Magnetic surveys are typically performed for:

- Geological Mapping - to aid in mapping lithology, structure, and alteration.
- Depth to Basement Mapping - for exploration in sedimentary basins or mineralization associated with the basement surface.

2.2 Radiometric Data

Radiometric surveys are used to determine either the absolute or relative amounts of uranium (U), thorium (Th), and potassium (K) in surface rocks and soils using natural radioactive emanations. Gamma radiation is utilized due to its greater penetration depth compared with alpha and beta radiation. Radiometric data are useful for mapping lithology, alteration, and structure as well as providing insights into weathering. For example, the natural radioactivity of igneous rocks generally increases with SiO_2 content and clay minerals tend to fix the natural radioelements.

Gamma rays are electromagnetic waves with frequencies between 10^{19} and 10^{21} Hz emitted spontaneously from an atomic nucleus during radioactive decay, in packets referred to as photons. The energy E transported by a photon is related to the wavelength λ or frequency ν by the formula:

$$E = h\nu = hc/\lambda$$

where: c is the velocity of light
h is Planck's constant (6.626×10^{-34} joule).

All detectable gamma radiation from Earth materials comes from the natural decay products of three primary radioelements: U, Th, and K. Each individual nuclear species (isotope) emits gamma rays at one or more specific energies, as shown in Figure 5. Of the three main natural radioactive elements, only potassium (^{40}K) emits gamma energy directly, at 1.46 MeV. Uranium (^{238}U) and thorium (^{232}Th) emit gamma rays through their respective decay series; ^{214}Bi at 1.76 MeV for uranium and ^{208}Tl at 2.61 MeV for thorium. Accordingly, the ^{214}Bi and ^{208}Tl measurements are considered equivalents for uranium (eU) and thorium (eTh), as the daughter products will be in equilibrium under most natural conditions.

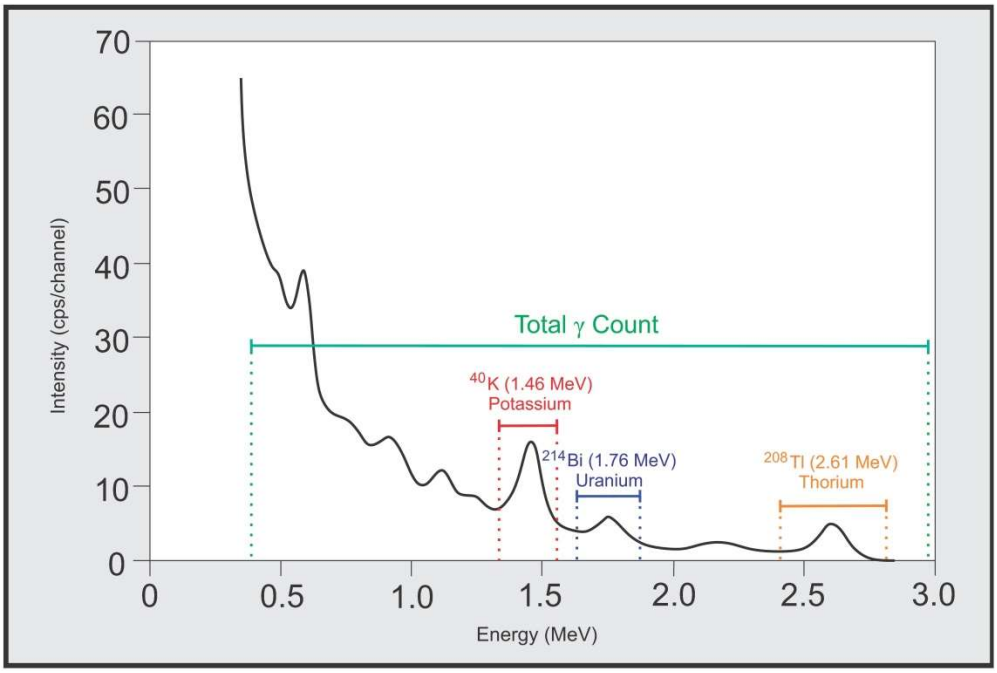

Figure 5: Typical natural gamma spectrum showing the three spectral windows (^{40}K 1.37-1.57 MeV, ^{214}Bi 1.66-1.86 MeV, ^{208}Tl 2.41-2.81 MeV) and total count (0.40-2.81 MeV) window.

Surficial debris, vegetation, standing water (lakes, marshes, swamps), and snow can effectively attenuate gamma rays originating from underlying rocks. Therefore, variations in isotope counts must be evaluated with respect to surficial conditions before they are attributed to changes in underlying geology. An increase in soil moisture can also significantly affect gamma radiation concentrations. For example, a 10% increase in soil moisture can decrease the measured gamma radiation by about the same amount. Radon isotopes are long-lived members of both the U and Th decay series and Ra mobility can influence radiometric surveys. In addition to being directly radioactive, ^{226}Ra and ^{222}Rn can attach to dust particles in the atmosphere. Radioactive precipitation of these dust particles by rain can lead to apparent increases of more than 2000% in uranium ground concentration (IAEA, 2003). Therefore, gamma ray surveying should not be carried out during a rainfall, or shortly after a rainfall.

3.0 Survey Operations

Survey operations began on July 4, 2018 and completed on July 5, 2018, in dry and windy conditions. The experience of the pilot ensured that the data quality objectives were met, and that the safety of the flight crew was never compromised given the potential risks involved in airborne geophysical surveying. Field processing and quality control checks were performed daily.

3.1 Operations Base and Crew

The base of operations was at Carmacks airport, Yukon (Figure 6) south of Golden Horseshoe survey block.

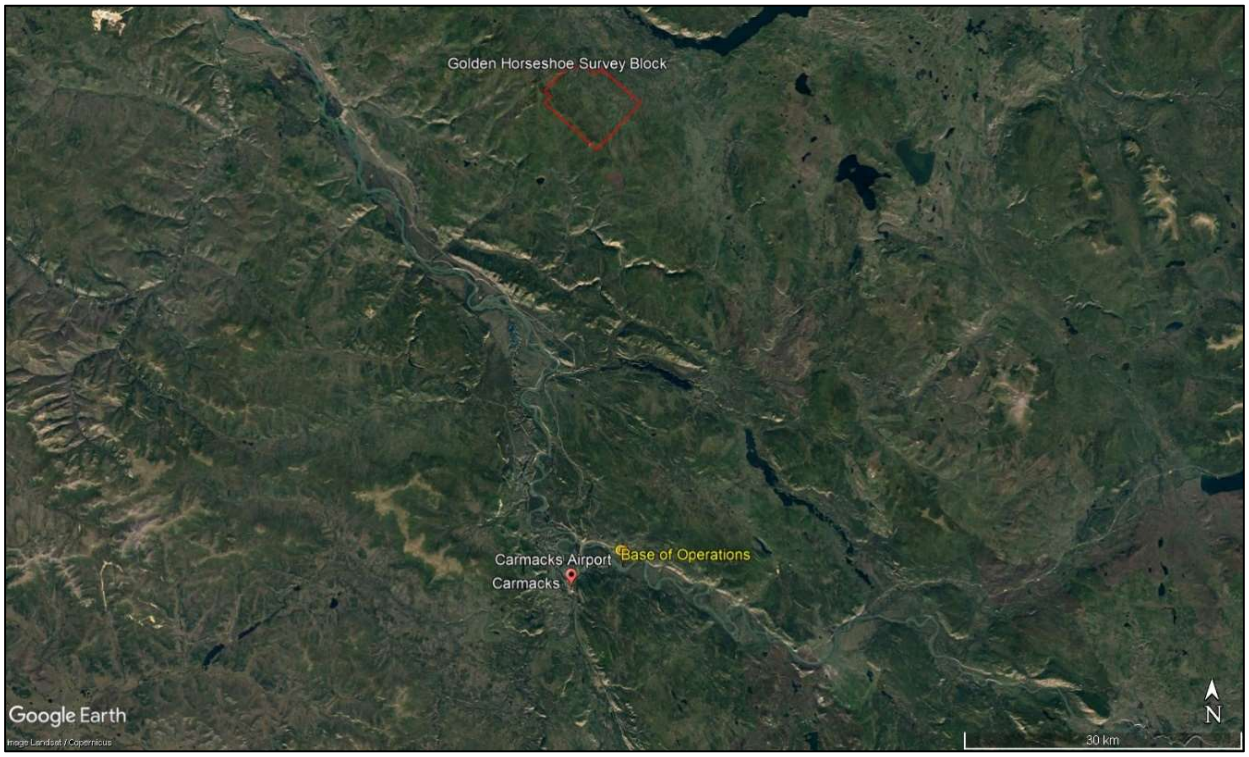

Figure 6: Map showing base of operations at Carmacks airport, Yukon south of Golden Horseshoe survey block.

The Precision geophysical crew consisted of four members (Table 3):

Crew Member	Position
Harmen Keyser, P.Geo.	Helicopter survey pilot
Bruce Larsen	Geophysical operator
Jenny Poon, B.Sc., P.Geo.	Geophysicist and data processor (off-site)
Shawn Walker, M.Sc., P.Geo.	Geophysicist and data processor (off-site)

Table 3: List of survey crew members.

3.2 Magnetic Base Station Specifications

Temporal magnetic field variations, such as diurnal variations, magnetic pulsations, and geomagnetic storms, were measured and recorded by two GEM GSM-19T proton precession magnetometers. The magnetic base stations were installed in an area (Table 4; Figures 7 and 8) of low magnetic noise away from metallic items such as ferromagnetic objects, vehicles, or power lines that could affect the base stations and ultimately the survey data.

Station name	Easting/Northing	Longitude/Latitude	Datum/ Projection
GEM 1 S/N 8052735	0437832E,6887534N	136° 11' 29.26" W 62° 06' 53.06" N	WGS 84, Zone 8N
GEM 2 S/N 2065369	0437841E,6887535N	136° 11' 28.64" W 62° 06' 53.10" N	WGS 84, Zone 8N

Table 4: Magnetic base station locations.

Magnetic readings were reviewed at regular intervals to ensure that no airborne data were collected during periods of high magnetic activity (greater than 10 nT change per minute).

Figure 7: GEM 1 and GEM 2 magnetic base stations located at Carmacks airport, Yukon.

Figure 8: GEM 1 (left) and GEM 2 (right) magnetic base stations located in the bushes at Carmacks airport, Yukon.

3.3 Field Processing and Quality Control

On a flight-by-flight basis, survey data were transferred from the aircraft's data acquisition system onto a USB memory stick and copied onto a field data processing laptop. The raw data files in PEI binary data format were converted into Geosoft GDB database format. Using Geosoft Oasis Montaj 9.3.3, the data were inspected to ensure compliance with contract specifications (Table 5; Figures 9 to 11).

Parameter	Specification	Tolerance
Position	Line Spacing	Flight line deviation within 10 m L/R from ideal flight path. No exceedance for more than 1 km.
	Height	Nominal flight height of 35 m AGL with tolerance of +/- 10 m. No exceedance for more than 1 km, provided deviation is not due to tall trees, topography, mitigation of wildlife/livestock harassment, cultural features, or other obstacles beyond the pilot's control.
	GPS	GPS signals from four or more satellites must be received at all times, except where signal loss is due to topography. No exceedance for more than 1 km.
Magnetics	Temporal/Diurnal Variations	Non-linear magnetic temporal variations within 10 nT of a linear chord of length 1 minute.
	Normalized 4th Difference	Magnetic data within 0.20 nT peak to peak. No exceedance for distances greater than 1 km or more, provided noise is not due to geological or cultural features.
Radiometrics	Test Line Data	Gamma signal from each of the four spectrometer windows (K, Th, U, TC) over the test line must be within 12%.

Table 5: Contract survey specifications.

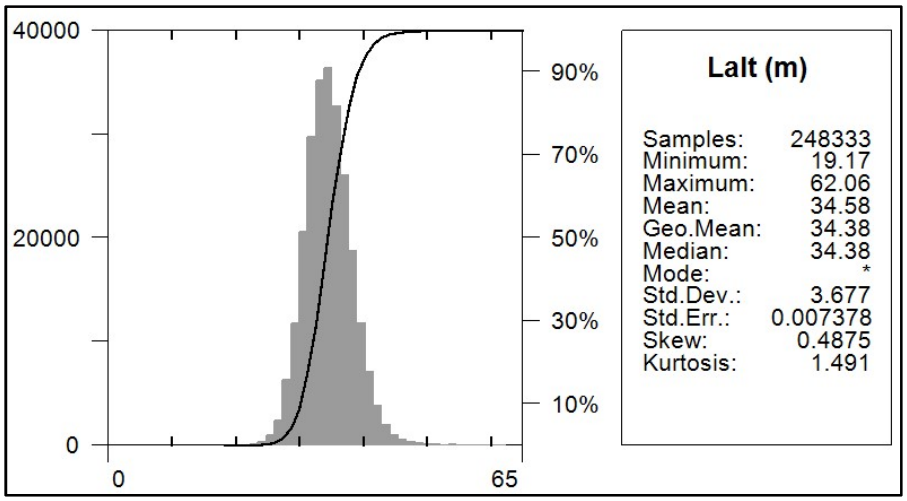

Figure 9: Histogram showing survey elevation vertically above ground.

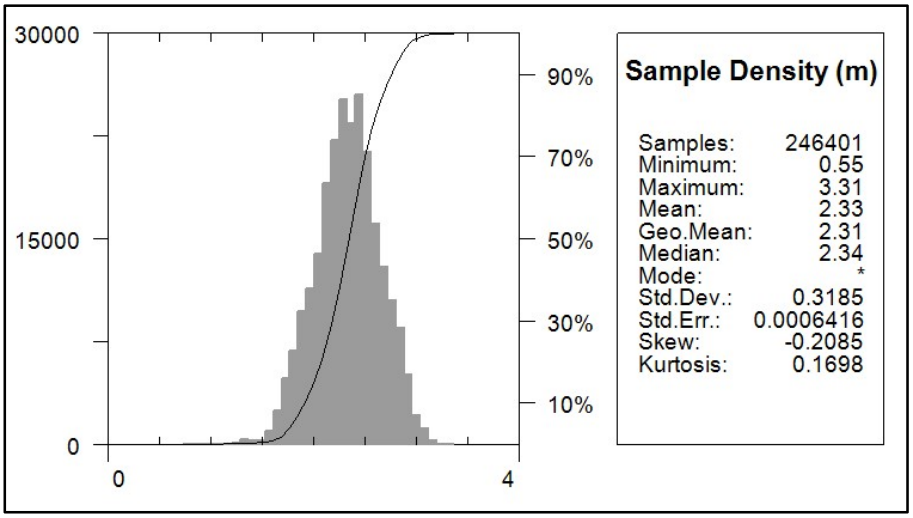

Figure 10: Histogram showing magnetic sample density. Linear distance in meters between adjacent measurement locations; magnetic sample frequency 20 Hz.

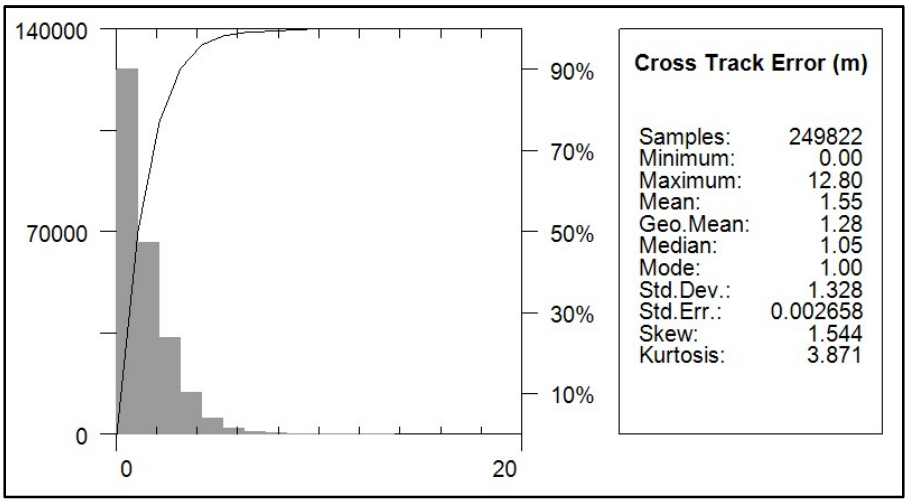

Figure 11: Histogram showing cross track error.

4.0 Aircraft and Equipment

All geophysical and subsidiary equipment were carefully installed on a Precision GeoSurveys aircraft to collect integrated magnetic and radiometric data.

4.1 Aircraft

Precision GeoSurveys flew the survey using an Airbus AS350 helicopter, registration C-GSVY, at a nominal height of 35 m AGL.

4.2 Geophysical Equipment

The survey aircraft (Figure 12) was equipped with a magnetometer, spectrometer, data acquisition system, laser altimeter, magnetic compensation system, barometer, temperature/humidity probe, pilot guidance unit (PGU), and GPS navigation system. In addition, two magnetic base stations were used to record temporal magnetic variations.

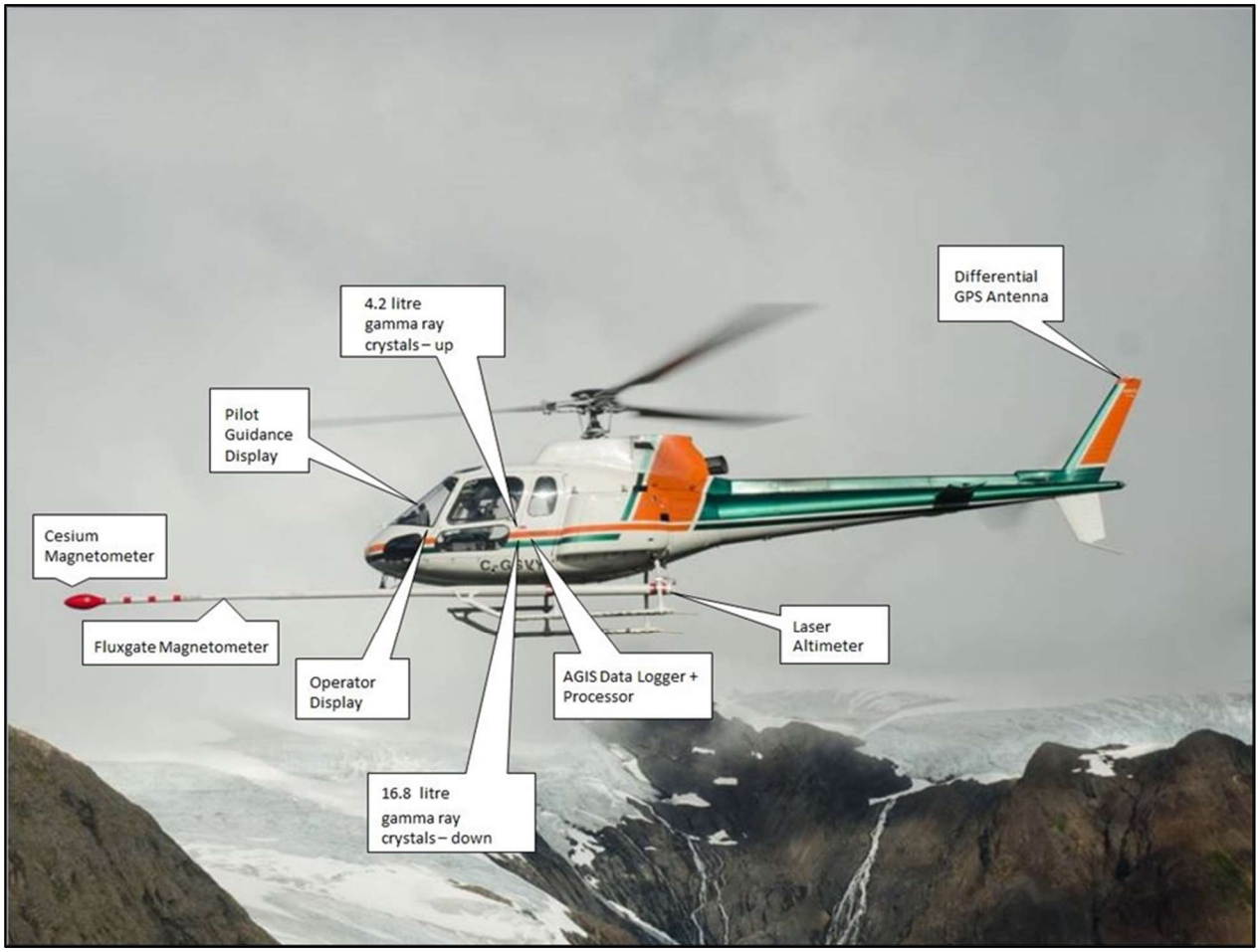

Figure 12: Survey helicopter equipped with geophysical equipment.

4.2.1 AGIS

The Airborne Geophysical Information System (AGIS), manufactured by Pico Envirotec, is the main computer used in integrated data recording, data synchronizing, displaying real-time quality control data for the geophysical operator (Figure 13) and the generation of navigation information for the pilot and operator display systems. Information such as magnetic field components, aircraft position, survey altitude, and survey speed are recorded to solid-state memory and can all be monitored on the on-board AGIS display for immediate quality control.

Figure 13: AGIS operator display installed in Airbus AS350 survey helicopter, with screen displaying real time flight line recording and navigation parameters. Additional windows display real time geophysical data to operator.

4.2.2 Magnetometer

A Scintrex CS-3 cesium vapor magnetometer (S/N 0706248) was used for this airborne survey. The CS-3 is a high sensitivity/low noise magnetometer with automatic hemisphere switching and a wide voltage range; the static noise rating for the unit is +/- 0.01 nT. Magnetic data were recorded at 20 Hz. A separate fluxgate magnetometer determined the aircraft's attitude (pitches, rolls, and yaws) relative to the inclination and declination of the Earth's magnetic field, which was necessary to remove magnetic noise created by movement of the aircraft through a compensation process. The magnetic sensors were mounted on the front of the helicopter in an approved non-magnetic and non-conductive "stinger" configuration (Figures 14 and 15) to reduce influence from the aircraft's magnetic field.

Figure 14: View of magnetic "stinger" installation on survey helicopter.

Figure 15: View of cesium vapor magnetometer. Sensor oriented 45° from vertical to couple with local magnetic field at the Golden Horseshoe survey block.

4.2.3 Spectrometer

The GRS-10 radiometric data acquisition system is a fully integrated gamma radiation detection system (Figure 16) containing a total of 21 litres of NaI(Tl) synthetic crystals; 16.8 litres downward-looking and 4.2 litres of upward-looking, with 256 channel output at 1 Hz sampling rate. The downward-looking crystals are designed to measure gamma rays from below the aircraft and are equipped with upward-shielding high density RayShield® gamma-attenuating

blankets to minimize cosmic and solar gamma noise. The upward-looking crystal measures cosmic and solar gamma radiation originating from above the survey aircraft and is shielded from terrestrial radiation by the downward-looking crystals. All crystals are installed in the rear cabin of the helicopter away from variable fuel cell gamma attenuation.

Figure 16: GRS-10 thallium-activated sodium iodide gamma spectrometer crystal packs. The open unit on the right shows two individual 4.2 litre gamma detectors.

4.2.4 Magnetic Base Station

To monitor and record the Earth's temporal magnetic field variations, particularly diurnal, Precision GeoSurveys operated two GEM GSM-19T base station magnetometers at all times while airborne data were being collected. The base stations were located in an area with low magnetic gradient, away from electric power transmission lines and moving ferrous objects, such as motor vehicles, that could affect the survey data integrity.

The GEM GSM-19T magnetometer (Figure 17) with integrated GPS time synchronization uses proton precession technology with a 1 Hz sampling rate. The GSM-19T has an absolute accuracy of +/- 0.2 nT and sensitivity of 0.15 nT at 1 Hz. Base station magnetic data were recorded on internal solid-state memory and downloaded onto a field laptop computer using a serial cable and GEMLink 5.4 software. Profile plots of the base station readings were generated, updated, and reviewed at the end of each survey day.

Figure 17: GEM GSM-19T proton precession magnetometer.

4.2.5 Laser Altimeter

Terrain clearance is measured by an Opti-Logic RS800 Rangefinder laser altimeter (Figure 18) attached to the aft end of the magnetometer boom. The RS800 laser is a time-of-flight sensor that measures distance by a rapidly modulated and collimated laser beam that creates a dot on the target surface. The maximum range of the laser altimeter is 700 m off natural surfaces with an accuracy of +/- 1 meter on 1 x 1 m diffuse target with 50% (+/- 20%) reflectivity. Within the sensor unit, reflected signal light is collected by the lens and focused onto a photodiode. Through serial communications and digital outputs, ground clearance data are transmitted to an RS-232 compatible port and recorded and displayed by the AGIS and PGU at 10 Hz in meters.

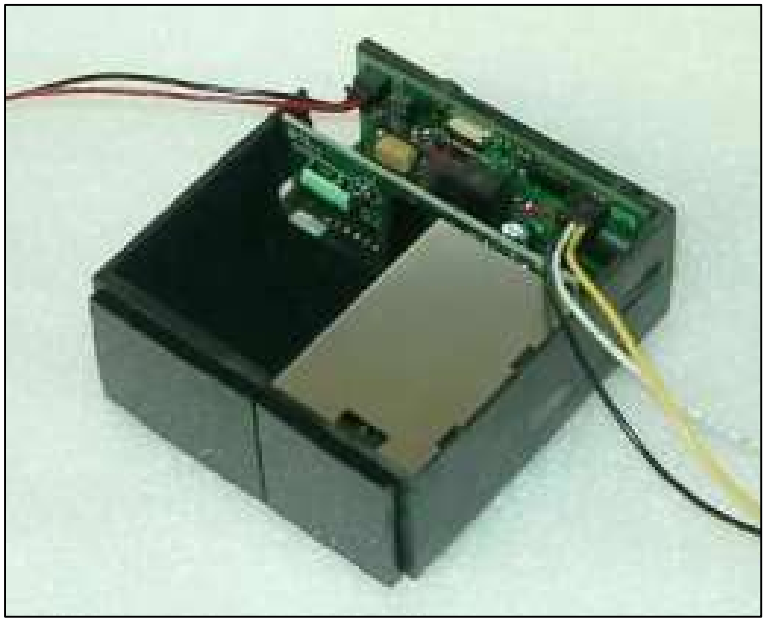

Figure 18: Opti-Logic RS800 Rangefinder laser altimeter.

4.2.6 Pilot Guidance Unit

Steering and elevation (ground clearance) information is continuously provided to the pilot by the Pilot Guidance Unit (PGU). The graphical display is mounted on top of the aircraft's instrument panel, remotely from the data acquisition system. The PGU is the primary navigation aid (Figure 19) to assist the pilot in keeping the aircraft on the planned flight path, heading, speed, and at the desired ground clearance.

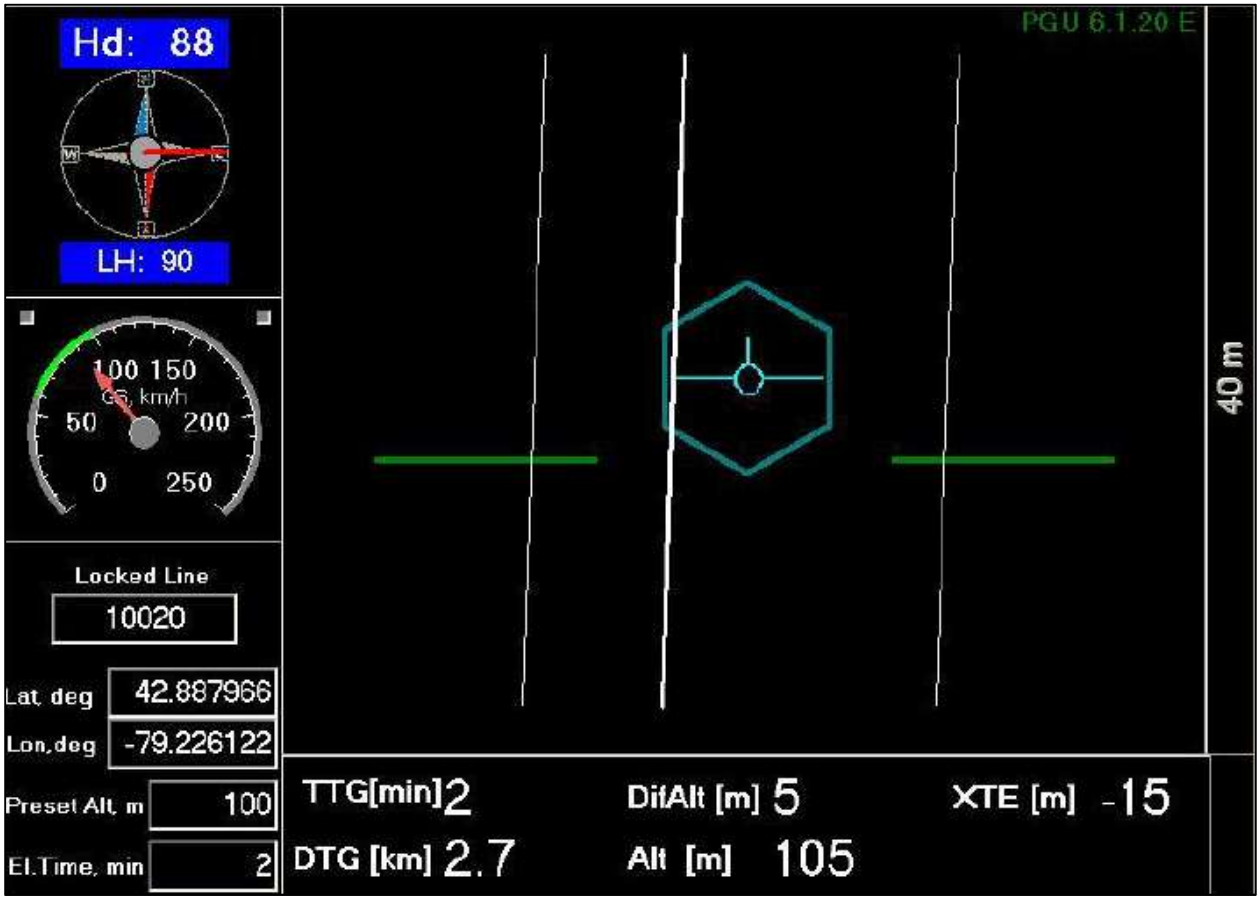

Figure 19: PGU screen displaying navigation information.

The LCD monitor measures 7 inches, with a full VGA 800 x 600 pixel display. The CPU for the PGU is contained in a PC-104 console and uses Microsoft Windows operating system control, with input from the GPS antenna, embedded drape surface profile or laser altimeter, and AGIS.

4.2.7 GPS Navigation System

A Hemisphere R120 GPS receiver (Figure 20) navigation system integrated with the pilot display (PGU) and AGIS provided navigational information and control. The R120 GPS receiver supports fast updates and outputs messages at a rate of up to 20 Hz (20 times per second); delivering sub-meter positioning accuracy in three dimensions. It employs COAST technology

that allows continuous operation for at least 40 minutes during temporary differential signal outages.

The receiver supports GPS, SBAS (Satellite-Based Augmentation System), and L-Band (OmniSTAR HP and XP) differential corrections to provide accurate positioning.

Figure 20: Hemisphere R120 GPS receiver.

5.0 Data Acquisition Equipment Checks and Calibration

Airborne equipment tests and calibrations were conducted for the laser altimeter, magnetometer, and spectrometer. A lag test was performed for all three sensors. There were two tests conducted for the airborne magnetometer: compensation flight and heading error test. There were three tests conducted for the gamma spectrometer: calibration pad test, cosmic flight test, and altitude correction and sensitivity test.

5.1 Lag Test

A lag test was performed to determine the relationship between the time the digital reading was recorded for the magnetometer, gamma spectrometer, and laser altimeter with the position fix time that the fiducial of the reading was obtained by the GPS system resulting from a combination of system lag and different locations of the sensors and the GPS antenna. The test was flown in the four orthogonal survey headings over an identifiable magnetic anomaly at survey speed and height. A lag of 2 fiducials (0.1 seconds) was determined for the magnetic sensor, a lag of 12 fiducials (0.6 seconds) was determined for the spectrometer, and a lag of 24 fiducials (1.2 seconds) was determined for the laser altimeter.

5.2 Magnetometer Tests

The magnetometer was tested and calibrated with a series of dedicated flights specifically for removing undesired effects of aircraft movement, speed, and heading direction.

5.2.1 Compensation Flight Test

During aeromagnetic surveying a small but significant amount of noise is introduced to the magnetic data by the aircraft itself, as the magnetometer is within the aircraft's magnetic field. Movement of the aircraft (roll, pitch, and yaw) combined with the permanent magnetization of certain aircraft parts (in particular the engine and other ferrous magnetic objects) contribute to this noise. The aircraft was degaussed using proprietary technology prior to starting the survey and the remaining magnetic noise was removed by a process called magnetic compensation.

A magnetic compensation flight was completed (Table 6). The process consists of a series of prescribed maneuvers where the aircraft flies in the four orthogonal headings required for the survey (043°/133°/223°/313° in the case of this survey) at a sufficient altitude (typically > 2,500 m AGL) in an area of low magnetic gradient where the Earth's magnetic field becomes nearly uniform at the scale of the compensation flight. In each heading direction, three specified roll, pitch, and yaw maneuvers (total 36) are performed by the pilot at constant elevation so that any magnetic variation recorded by the airborne magnetometer can be attributed to aircraft movement. These maneuvers are recorded by the airborne fluxgate magnetometer and provide the data that are required to calculate the necessary parameters for compensating the magnetic data to remove aircraft noise from survey data.

Pre-Compensation					Post-Compensation				
Heading	**Roll**	**Pitch**	**Yaw**	**Total**	**Heading**	**Roll**	**Pitch**	**Yaw**	**Total**
043°	3.4647	1.3315	0.9547	5.7509	043°	0.1987	0.2085	0.1971	0.6043
133°	3.9903	1.0929	0.9019	5.9851	133°	0.1546	0.2013	0.2014	0.5573
223°	3.5996	1.6827	1.1354	6.4177	223°	0.2133	0.2401	0.1961	0.6495
313°	3.0076	1.1200	0.6726	4.8002	313°	0.1624	0.1735	0.1496	0.4855
Total	14.0622	5.2271	3.6646		**Total**	0.7290	0.8234	0.7442	
FOM (nT) = 22.9539					**FOM (nT) = 2.2966**				

Table 6: Figure of Merit maneuver test results for 043°/133°/223°/313° compensation flight flown on July 5, 2018.

5.2.2 Heading Error Test

To determine the magnetic heading effect a cloverleaf pattern flight test was conducted. The cloverleaf test was flown in the same orthogonal headings (Table 7) as the survey and tie lines (043°/133°/223°/313°) at >1000 m AGL in an area with low magnetic gradient. For the cloverleaf test, the survey aircraft must pass over the same mid-point all four times at the same elevation so that any change in measured magnetic intensity can be attributed to heading.

Heading	Fiducial	Mag (nT)	Correction (nT)
043°	9259.3	56821.18	-1.55
133°	8839.8	56826.65	-7.02
223°	9151.4	56816.91	2.72
313°	9013.3	56813.78	5.85
	Average	56819.63	
	Total		0.0000

Table 7: Heading error test data format flown on July 5, 2018.

5.3 Gamma-ray Spectrometer Tests and Calibrations

Calibration and testing of the GRS-10 airborne gamma-ray spectrometry system was carried out prior to the start of the survey. The calibration of the spectrometer system involved three tests which enabled the conversion of airborne data to ground concentration of natural radioactive elements. These tests were the calibration pad test, cosmic flight test, and the altitude correction and sensitivity test. Measurements were made in accordance with IAEA technical report series No. 323, *Airborne Gamma Ray Spectrometer Surveying*, and AGSO Record 1995/60, *A Guide to the Technical Specifications for Airborne Gamma-Ray Surveys*.

5.3.1 Calibration Pad Test

The calibration pad test was conducted by Pico Envirotec using GSC (Geological Survey of Canada) portable calibration pads. The pads are slabs of concrete containing known concentrations of the radioelements (K, Th, and U) and are used to simulate ideal geological sources of radiation. The measurements collected from the calibration pad test were used to determine the Compton scattering and Grasty backscatter (spectral overlap between element windows) coefficients.

5.3.2 Cosmic Flight Test

While the background source of gamma radiation from the aircraft itself is essentially constant, the amount of signal detected from ground sources varies with ground clearance. As the height of the aircraft increases, the distance between the ground and the spectrometer crystals increases, and the proportion of cosmic radiation in each spectral window increases exponentially due to radiation of cosmic origin. The cosmic flight test is conducted to determine the aircraft's background attenuation coefficients for the detector crystal packs and the cosmic coefficients. The pilot is required to fly over the same location repeatedly in opposite directions at the following elevations in meters above

ground; 900, 1500, 2100, 2400, and 2700, for approximately 2 minutes each to collect gamma data used to determine the amount of non-terrestrial gamma signal.

5.3.3 Altitude Correction and Sensitivity Test

The altitude and sensitivity test is similar to the cosmic flight test but is conducted at lower elevations (from ground level). The pilot is required to fly over the same location at the following elevations in meters above ground; 30, 60, 90, 120, 150, 210, 270, and 360, for 2 minutes each. As the distance of the aircraft increases away from the radioactive ground source, the source signature exponentially degrades. As a result, this test is used to determine the altitude attenuation coefficients and the radio-element sensitivity of the airborne spectrometer system.

6.0 Data Processing

After all data were collected, several procedures were undertaken to ensure that the data met a high standard of quality. All magnetic and radiometric data recorded by the AGIS are converted into Geosoft or ASCII file formats by using Pico Envirotec software. Further processing (Figure 21) was carried out using Geosoft Oasis Montaj 9.3.3 geophysical processing software along with proprietary processing algorithms.

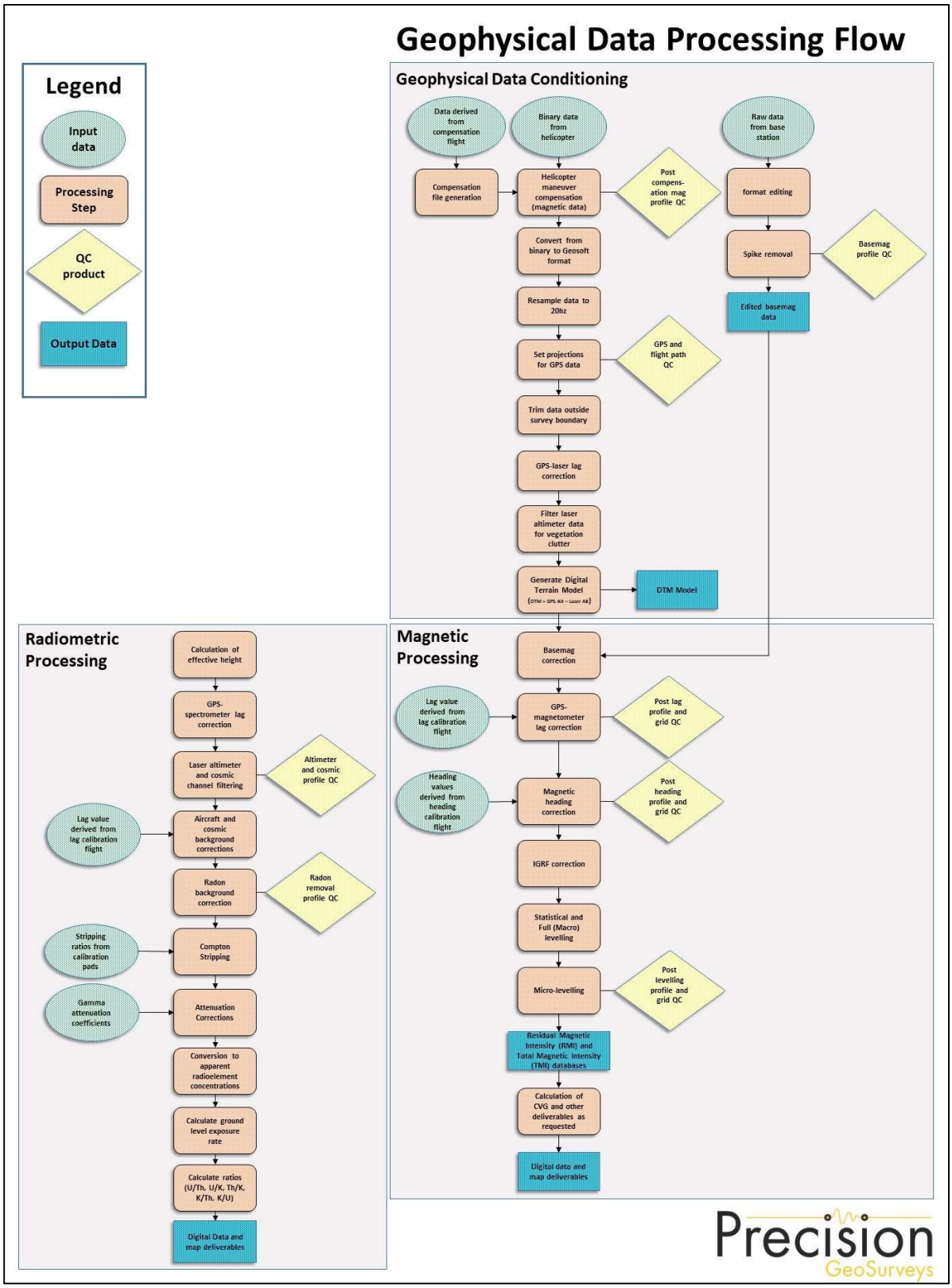

Figure 21: Magnetic and radiometric data processing flow.

6.1 Flight Height and Digital Terrain Model

A lag correction of 1.2 seconds was applied to the raw laser data to compensate for the combination of lag in the recording system and the difference in position of the laser altimeter and the GPS antenna.

Laser altimeters cannot provide valid data over glassy water, fog, or dense vegetation. Over areas with dense vegetation a certain proportion of the laser signal does not penetrate through the trees to record actual ground clearance and high frequency variations are recorded. A Rolling Statistics filter was applied to the laser data to remove vegetation clutter followed by a Low Pass filter which was used to smooth out the laser altimeter profile to eliminate isolated high frequency noise and generate a surface closely corresponding to the actual ground profile.

A Digital Terrain Model (DTM) channel was calculated by subtracting the processed laser altimeter data from the filtered GPS altimeter data defined by the WGS 84 ellipsoidal height. The accuracy of the DTM is affected by the geometric relationship between the GPS antenna, the laser altimeter, flight attitude of the aircraft, and the slope of the ground as well as sample density.

6.2 Magnetic Processing

Raw magnetic data, as collected by the airborne instruments, were corrected for flight maneuvers, temporal variations, lag, and heading. The data were examined for magnetic noise and spikes, which were removed as required. Survey and tie line data of the resulting total magnetic field were leveled and the background magnetic field, International Geomagnetic Reference Field of the Earth, removed.

6.2.1 Flight Compensation

Data obtained from the compensation flight test were applied to the raw magnetic data as the first step of data processing. A computer program called PEIComp was used to create a model from the compensation flight test for each survey to remove the noise induced by aircraft movement; this model was applied to data from each survey flight.

6.2.2 Base Station Correction

The next step in processing the compensated magnetic data was to correct for temporal variation of the Earth's magnetic field. Magnetic data from base station GEM 1 were used for correcting the airborne magnetic survey data, and GEM 2 data were retained for backup. The data were edited, plotted, and merged into a Geosoft database (.GDB) on a daily basis.

The base station measurements were averaged to establish a magnetic base reference datum at 56734.58 nT, and this value was used to calculate the observed magnetic base station deviations resulting from variations of the Earth's magnetic field over time with reference to the datum. The

airborne magnetic data were then corrected for temporal variations by subtracting the base station deviations from the data collected on the aircraft, which effectively removed the effects of diurnal and other temporal variations.

6.2.3 Lag Correction

Following the base station correction, a lag correction of 0.1 seconds was applied to each total magnetic field data point to compensate for the combination of lag in the recording system and the magnetometer sensor flying 14.7 m ahead of the GPS antenna.

6.2.4 Heading Correction

For each survey heading, changes in instrument magnetic fields along a survey flight line are detected and these systematic shifts are recorded. These values are used to construct a heading .TBL table file. An intersection table was created, containing all magnetic field values where tie lines intersected the survey lines and the overall average magnetic field value was calculated. For each of the four headings, the averages were calculated and then compared to the overall average to determine four values to be used for heading error correction.

6.2.5 IGRF Removal

The International Geomagnetic Reference Field (IGRF) model is the empirical representation of the Earth's magnetic field (main core field without external sources) collected and disseminated from satellite data and from magnetic observatories around the world. The IGRF is generally revised and updated every five years by a group of modelers associated with the International Association of Geomagnetism and Aeronomy (IAGA). Accordingly, the 12th generation IGRF (IGRF-12), an IGRF model for epoch 2015.0 was used with the actual survey date obtained from the "Date" channel.

Residual Magnetic Intensity (RMI) was calculated by taking the difference between IGRF and the non-leveled Total Magnetic Intensity (TMI). This created a more valid model of individual near-surface anomalies so that the data were not referenced to a specific time. This will allow for other magnetic data (historic or future) to be more easily incorporated into each survey database.

6.2.6 Leveling and Micro-leveling

Residual Magnetic Intensity (RMI) data from survey and tie lines were used to level the entire survey dataset. Two types of leveling were applied to the corrected data: conventional leveling and micro-leveling. There were two components to conventional leveling; statistical leveling to level tie lines and full leveling to level survey lines. The statistical leveling method corrected the SL/TL intersection errors that follow a specific pattern or trend. Through the error channel, an algorithm calculated a least-squares trend line and derived a trend error curve, which was then added to the channel to be leveled. The second component was full leveling. This adjusted the

magnetic value of the survey lines so that all lines matched the trended tie lines at each intersection point.

Following statistical leveling, micro-leveling was applied to the corrected conventional leveled data. This iterative grid-based process removed low amplitude components of flight line noise that still remained in the data after tie line and survey line leveling and resulted in fully leveled RMI data. The IGRF was then added back onto the RMI to allow for the production of a leveled TMI grid and map.

6.2.7 Reduced to Magnetic Pole

Reduced to Magnetic Pole (RTP) data were computed from the leveled Residual Magnetic Intensity (RMI) data. The RTP filter was applied in the Fourier domain and it migrates the observed magnetic inclination and declination field to what the field would look like at the north magnetic pole.

6.2.8 Calculation of First Vertical Derivative

The first vertical derivative was computed from the leveled Residual Magnetic Intensity (RMI) data. The first vertical derivative calculates the vertical rate of change in the magnetic field. It is used to enhance shorter wavelength signals; therefore, edges of magnetic anomalies are highlighted, and deep geologic sources in the data are suppressed.

The first vertical derivative calculated from the RMI was designated as Calculated Vertical Derivative of RMI, or CVG.

Vertical derivative to the nth derivative is:

$$L(r) = r^n$$

6.2.9 Calculation of Horizontal Gradient

The Calculated Horizontal Gradient (CHG) is the magnitude of the total horizontal gradient. It is used to estimate contact locations of magnetic bodies at shallow depths, reveal anomaly texture, and highlight anomaly-pattern discontinuities.

If M is the magnetic field, then the CHG is calculated as:

$$\mathrm{CHG}(x, y) = \sqrt{\left(\frac{\partial M}{\partial x}\right)^2 + \left(\frac{\partial M}{\partial y}\right)^2}$$

6.3 Radiometric Processing

Radiometric surveys map gamma rays from the concentration of radioelements at or near Earth's surface; typically, up to 1.5 meters below surface. Before any processing of the airborne radiometric data, the spectrometer system is calibrated with the calibration pad test, cosmic flight test, and altitude correction and sensitivity test. Once calibration of the system was complete, the radiometric data were processed by windowing the full spectrum to create individual channels for U, Th, K, and total count.

Steps taken to process acquired radiometric data are summarized below:

- Calculation of effective height
- Lag Correction
- Aircraft and Cosmic background corrections
- Radon background correction
- Stripping ratios
- Attenuation corrections
- Conversion to apparent radioelement concentrations

6.3.1 Calculation of Effective Height

Laser/Radar altimeter data were converted to effective height (h_{ef}) in meters using the acquired laser/radar altimeter, temperature and pressure data, according to the formula below:

$$h_{ef} = h * \frac{273.15}{T + 273.15} * \frac{P}{1013.25}$$

where: h is observed laser/radar altitude in meters
T is measured air temperature in degrees Celsius
P is barometric pressure in millibars

6.3.2 Lag Correction

Following the calculation of effective height, a lag correction of 0.6 seconds was applied to each radiometric channel to compensate for the combination of lag in the recording system and the difference in position of the spectrometer and the GPS antenna.

6.3.3 Aircraft and Cosmic Background Corrections

Aircraft background and cosmic stripping corrections are applied to all three elements, and total count, using the following formula:

$$C_{ac} = \mathrm{a}_c + b_c * Cos_f$$

where: C_{ac} is the background and cosmic corrected channel
a_c is the aircraft background for this channel
b_c is the cosmic stripping coefficient for this channel
Cos_f is the filtered cosmic channel

6.3.4 Radon Background Correction

To strip the effects of atmospheric radon from the downward-looking detectors, there are multiple methods available for radon background estimation. The method selected was the background table method. Procedures to the background table method and how to determine the radiometric values filled within the table in detail are outlined in the IAEA 1363 report, *Guidelines for Radioelement Mapping using Gamma Ray Spectrometry Data*.

6.3.5 Compton Stripping

Spectral overlap corrections are applied to potassium, uranium, and thorium as part of the Compton stripping process. This is done by using the stripping ratios that have been calculated for the spectrometer by prior calibration; this breaks the corrected elemental values down into the apparent radioelement concentrations.

Stripping ratios α, β, and γ are first modified according to altitude. Then an adjustment factor (derived from the cosmic flight test), the reversed stripping ratio, uranium into thorium, is calculated.

$$\alpha_h = \alpha + h_{ef} * 0.00049$$

$$\beta_h = \beta + h_{ef} * 0.00065$$

$$\gamma_h = \gamma + h_{ef} * 0.00069$$

where: $\alpha, \beta. \gamma$ are the Compton stripping coefficients
$\alpha_h, \beta_h. \gamma_h$ are the height corrected Compton stripping coefficients
h_{ef} is the effective height above ground in metres at STP

The stripping corrections are then carried out using the following formulas:

$$Th_c = Th_{bc}(1 - g\beta_h) + U_{bc}(b\gamma_h - a) + K_{bc}(ag - b)/A$$

$$U_c = Th_{bc}(g\beta_h - \alpha_h) + U_{bc}(1 - b\beta_h) + K_{bc}(b\alpha_h - g)/A$$

$$K_c = [Th_{bc}(\alpha_h\gamma_h - \beta_h) + U_{bc}(a\beta_h - \gamma_h) + K_{bc}(1 - a\alpha_h)]/A$$

where: $U_c, Th_c,$ and K_c are stripping corrected uranium, thorium and potassium

α_h, β_h. γ_h are height corrected Compton stripping coefficients
U_{bc}, Th_{bc}, and K_{bc} are background corrected uranium, thorium and potassium
a is the spectral ratio Th/U
b is the spectral ratio Th/K
g is the spectral ratio U/K
$A = 1 - g\gamma_h - (\alpha_h - g\,\beta_h) - b(\beta_h - \alpha_h\,\gamma_h)$ is the backscatter correction

6.3.6 Attenuation Corrections

The total count, potassium, uranium, and thorium data are then corrected to a nominal survey altitude (corrected to remove vegetation clutter from radar/laser altimeter data), in this case the survey height was 35 meters. This is done according to the equation:

$$C_a = C * e^{\mu(h_{ef} - h_0)}$$

where: C_a is the output altitude corrected channel
C is the input channel
μ is the attenuation correction for that channel
h_{ef} is the effective altitude, usually in m
h_0 is the nominal survey altitude used as datum

6.3.7 Conversion to Apparent Radioelement Concentrations

With all corrections applied to the radiometric data, the final step is to convert the corrected potassium (^{40}K), uranium (from ^{214}Bi), and thorium (from ^{212}Tl) to apparent radioelement concentrations using the following formula:

$$eE = C_{cor}/S$$

where: eE is the element concentration K(%) and equivalent element concentration of U (ppm) & Th (ppm)
S is the experimentally determined sensitivity
C_{cor} is the fully corrected channel

Finally, the natural air exposure rate is determined by using the following formula:

$$E = [(13.08 * K + 5.43 * eU + 2.69 * eTh)/8.69]$$

where: E is the absorption dose rate in µR/h
K is the concentration of potassium (%)
eU is the equivalent concentration of uranium (ppm)
eTh is the equivalent concentration of thorium (ppm)

6.3.8 Radiometric Ratios

To calculate some of the common radiometric ratios (U/Th, Th/K, and U/K and their inverses) the guidelines of the IAEA are followed. Due to statistical uncertainties in the individual radioelement measurements, care is taken during ratio calculation in order to obtain statistically significant values. Following IAEA guidelines, the method of determining ratios of the eU/eTh, eU/K and eTh/K is as follows:

1. Any data points where the potassium concentration is less than 0.25% are neglected.
2. The element with the lowest corrected count rate is determined.
3. The element concentrations of adjacent points on either side of each data point are summed until they exceed a pre-determined threshold value. This threshold is set to be equivalent to 100 counts of the element with the lowest count rate. Additional minimum thresholds of 1.6% for potassium, 20 ppm for thorium, and 30 ppm for uranium are established to ensure meaningful ratios.
4. The ratios are calculated using the accumulated sums.

With this method, errors associated with the calculated ratios are minimized and comparable for all data points.

7.0 Deliverables

Survey data are presented as digital databases, maps, and a logistics report.

7.1 Digital Data

The digital files have been provided in two formats, the first is a .GDB file for use in Geosoft Oasis Montaj and the second format is a .XYZ (text) file. Full descriptions of the digital data and contents are included in the report (Appendix B).

The digital data were represented as grids, as listed below:

- Digital Terrain Model (DTM)
- Total Magnetic Intensity (TMI)
- Residual Magnetic Intensity (RMI) – removal of IGRF from TMI
- Calculated Vertical Gradient (CVG) - first vertical derivative of RMI
- Reduced to Magnetic Pole (RTP) – reduced to magnetic pole of RMI
- Calculated Horizontal Gradient (CHG) – total horizontal gradient of RMI
- Potassium – Equivalent Concentration in Percentage (%K)
- Thorium – Equivalent Concentration (eTh)
- Uranium – Equivalent Concentration (eU)
- Total Count – Equivalent Dose Rate (TCcor)

- Total Count – Exposure Rate (TCexp)
- Potassium over Thorium Ratio (%K/eTh)
- Potassium over Uranium Ratio (%K/eU)
- Uranium over Thorium Ratio (eU/eTh)
- Uranium over Potassium Ratio (eU/%K)
- Thorium over Potassium Ratio (eTh/%K)
- Thorium over Uranium Ratio (eTh/eU)
- Ternary Map (TM)

7.1.1 Grids

Digital data were gridded and displayed using the following Geosoft parameters:

- Grid cell size: 25 m
- % pass tolerance: 99
- Maximum iterations: 100

All grids were drawn with a histogram-equalized color shade; sun illumination inclination at 45° and declination at 045°.

7.2 KMZ

The digital data represented as grids were exported into .kmz files which can be displayed using Google Earth. The grids can be draped onto topography and rendered to give a 3D view.

7.3 Maps

Digital maps were created for Golden Horseshoe survey block. The following map products were prepared:

Overview Maps (colour images with elevation contour lines):

- Actual flight lines, with property boundaries
- DTM

Magnetic Maps (colour images with elevation contour lines):

- TMI with actual flight lines
- TMI
- RMI
- CVG of RMI
- RTP of RMI
- CHG of RMI

Radiometric Maps (colour images with elevation contour lines):

- %K – Equivalent Concentration in Percentage
- eTh – Equivalent Concentration
- eU – Equivalent Concentration
- TCcor – Equivalent Dose Rate
- TCexp – Exposure Rate
- %K/eTh Ratio
- %K/eU Ratio
- eU/eTh Ratio
- eU/%K Ratio
- eTh/%K Ratio
- eTh/eU Ratio
- Ternary Map

All survey maps were prepared in WGS 84 and UTM zone 8N.

7.4 Report

A pdf copy of the logistics report is included along with the digital data and maps. The report provides information on the data acquisition procedures, magnetic and radiometric processing, and presentation of the Golden Horseshoe survey block data.

8.0 Conclusions and Recommendations

While the objective of geophysical data processing is to accurately represent the Earth's geophysical features, continual processing, such as the calculation of derivatives, can generate false features as the signal-to-noise ratio decreases. In addition, false features can appear near the edges of a survey block where gridding algorithms are unable to properly calculate grids, such as in "edge effects." Therefore, subtle geophysical features in derivative-enhanced map products or near the survey margins must be used with discretion.

The airborne geophysical data were acquired to map the geophysical characteristics of the survey area, which are in turn related to the distribution and concentration of magnetic minerals and radioactive elements in the Earth. Geophysical data are not a direct indication of mineral deposits and therefore interpretation and careful integration with existing and new geological, geochemical, and other geophysical data are recommended to maximize value from the survey investment.

Appendix A

Equipment Specifications

- GEM GSM-19T Proton Precession Magnetometer (Magnetic Base Station)
- Hemisphere R120 GPS Receiver
- Opti-Logic RS800 Rangefinder Laser Altimeter
- Setra Model 276 Barometric Pressure
- Scintrex CS-3 Survey Magnetometer
- Billingsley Mag-03 three-axis fluxgate magnetic field sensor
- Pico Envirotec GRS-10 Gamma Spectrometer
- Pico Envirotec AGIS data recorder system (for navigation and geophysical data acquisition)

GEM GSM-19T Proton Precession Magnetometer (Magnetic Base Station) Specifications

Configuration Options	15
Cycle Time	999 sec to 0.5 sec
Environmental	-40°C to +60°C
Gradient Tolerance	7,000 nT/m
Magnetic Readings	299,593
Operating Range	10,000 to 120,000 nT
Power	12 V @ 0.62 A
Sensitivity	0.1 nT @ 1 sec
Absolute accuracy	1 nT
Weight (Console/Sensor)	3.2 Kg
Integrated GPS	Yes

Hemisphere R120 GPS Receiver Specifications

GPS Sensor	Receiver Type	L1, C/A code, with carrier phase smoothing (Patented COAST technology during differential signal outage
	Channels	12-channel, parallel tracking (10-channel when tracking SBAS)
	Update Rate	Up to 20 Hz position
	Cold Start Time	<60 s
	SBAS Tracking	2-channel, parallel tracking
	Horizontal Accuracy	<0.02 m 95% confidence (RTK 1, 2) <0.28 m 95% confidence (L-Dif 1, 2) <0.6 m 95% confidence (DGPS 1,3) <2.5 m 95% confidence (autonomous, no SA1)
	Differential Options	SBAS, Autonomous, External RTCM, RTK, OmniSTAR (HP/XP)
Beacon Sensor Specifications	Channels	2-channel, parallel tracking
	Frequency Range	283.5 to 325 kHz
	MSK Bit Rates	50, 100, and 200 bps
L-Band Sensor	Channels	Single channel
	Frequency Range	1530 MHz to 1560 MHz
	Satellite Selection	Manual or Automatic (based on location)
	Startup and Satellite Reacquisition Time	15 seconds typical
Communications	Serial Ports	2 full duplex RS232C
	Baud Rates	4800 – 115200
	USB Ports	1 Communications
	Correction I/O Protocol	RTCM SC-104
	Data I/O Protocol	NMEA 0183
	Timing Output	1 PPS (HCMOS, active high, rising edge sync, 10 kΩ, 10 pF load)
	Raw Data	Proprietary binary (RINEX utility available)
Environmental	Operating Temperature	-30°C to +70°C
	Storage Temperature	-40°C to +85°C
	Humidity	95% non-condensing
Power GPS Sensor	Input Voltage Range	8 to 36 VDC
	Power Consumption	3 Watts
	Current Consumption	< 250 mA @ 12 VDC
	Antenna Voltage Output	5.0 VDC

[1]Depends on multipath environment, number of satellites in view, satellite geometry and ionospheric activity.
[2] Up to 5 km baseline length.
[3] Depends also on baseline length.

Opti-Logic RS800 Rangefinder Laser Altimeter Specifications

Accuracy	+/- 1 m on 1x1 m^2 diffuse target with 50% reflectivity, up to 700 m
Resolution	0.2 m
Communication Protocol	RS232-8,N,1
Baud Rate	19200
Data Raw Counts	~200 Hz
Data Calibrated Range	~10 Hz
Calibrated Range Units	Feet, Meters, Yards
Laser	Class I (eye-safe) 905 nm +/- 10 nm
Power	7-9 VDC conditioned required, current draw at full power (~ 1.8 W)
Laser Wavelength	RS100 905 nm +/- 10 nm
Laser Divergence	Vertical axis – 3.5 mrad half-angle divergence; Horizontal axis – 1 mrad half-angle divergence; (Approximate beam footprint at 100 m is 35 cm x 5 cm)
Data Rate	~200 Hz raw counts for un-calibrated operation; ~10 Hz for calibrated operation (averaging algorithm seeks 8 good readings)
Dimensions	32 x 78 x 84 mm (lens face cross section is 32 x 78 mm)
Weight	< 227 g (8 oz)
Casing	RS100/RS400/RS800 units are supplied as OEM modules consisting of an open chassis containing optics and circuit boards. Custom housings can be designed and built on request.

Setra Model 276 Barometric Pressure Specifications

Pressure Ranges	600 to 1100 hPa/mb 800 to 1100 hPa/mb 0 to 20 psia
Accuracy	±0.25% FS
Output	0.1 to 5.1 VDC 0.5 to 4.5 VDC
Excitation	12 VDC (9.0 to 14.5) 24 VDC (21.6 to 26.0) 5 VDC (4.9 to 7.1)
Size	2” dia. x 1” (5 cm x 2.5 cm)

Scintrex CS-3 Magnetometer Specifications

Operating Principal	Self-oscillation split-beam Cesium Vapor (non-radioactive Cs-133)
Operating Range	15,000 to 105,000 nT
Gradient Tolerance	40,000 nT/meter
Operating Zones	10° to 85° and 95° to 170°
Hemisphere Switching	a) Automatic b) Electronic control actuated by the control voltage levels (TTL/CMOS) c) Manual
Sensitivity	0.0006 nT √Hz rms
Noise Envelope	Typically 0.002 nT P-P, 0.1 to 1 Hz bandwidth
Heading Error	+/- 0.25 nT (inside the optical axis to the field direction angle range 15° to 75° and 105° to 165°)
Absolute Accuracy	<2.5 nT throughout range
Output	a) Continuous signal at the Larmor frequency which is proportional to the magnetic field (proportionality constant 3.49857 Hz/nT) sine wave signal amplitude modulated on the power supply voltage b) Square wave signal at the I/O connector, TTL/CMOS compatible
Information Bandwidth	Only limited by the magnetometer processor used
Sensor Head	Diameter: 63 mm (2.5”) Length: 160 mm (6.3”) Weight: 1.15 kg (2.6 lb)
Sensor Electronics	Diameter: 63 mm (2.5”) Length: 350 mm (13.8”) Weight: 1.5 kg (3.3 lb)
Cable, Sensor to Sensor Electronics	3 m (9’ 8”), lengths up to 5 m (16’ 4”) available
Operating Temperature	-40°C to +50°C
Humidity	Up to 100%, splash proof
Supply Power	24 to 35 Volts DC
Supply Current	Approx. 1.5 A at start up, decreasing to 0.5 A at 20°C
Power Up Time	Less than 15 minutes at -30°C

Billingsley Mag-03 three-axis fluxgate magnetic field sensor Specifications

Number of Axes	3
Bandwidth	0 to 3 kHz at 50 µT peak
Internal Noise	Basic version: >10 to 20 pTrms/√Hz at 1 Hz Standard version: 6 to ≤10 pTrms/√Hz at 1 Hz Low Noise version: <6 pTrms/√Hz at 1 Hz
Scaling error (DC)	<±0.5%
Orthogonality error	<0.1°
Alignment error (Z axis to reference face)	<0.1°
Linearity error	<0.0015%
Frequency response	0 to 1 kHz maximally flat, ±5% maximum at 1 kHz
Input voltage	±12 V to ±17 V
Supply current	+30 mA, -10 mA (+1.4 mA per 100 µT for each axis)
Power supply rejection ratio	5 µV/V (-106 dB)
Analog output	±10 V (±12 V supply) swings to within 0.5 V of supply voltage
Output impedance	10 Ω
Operating temperature range	-40°C to +70°C
Environmental protection	IP51
Dimensions (W x H x L)	32 x 32 x 152 mm
Weight	160 g
Enclosure material	Reinforced epoxy
Connector	ITT Cannon DEM-9P-NMB
Mating connector	ITT Cannon DEM-9S-NMB
Mounting	2 x M5 fixing holes

Pico Envirotec GRS-10 Gamma Spectrometer Specifications

Crystal volume	16.8 litres of NaI(Tl) synthetic downward-looking crystals and 4.2 litre NaI(Tl) synthetic upward-looking crystal
Resolution	256/512 channels
Tuning	Automatic using peak determination algorithm
Detector	Digital Peak
Calibration	Fully automated detector
Real Time	Linearization and gain stabilization
Communication	RS232
Detectors	Expandable to 10 detectors and digital peak
Count Rate	Up to 60,000 cps per detector
Count Capacity per channel	65545
Energy detection range:	36 KeV to 3 MeV
Cosmic channel	Above 3 MeV
Upward Shielding	RayShield® non-radioactive shielding on downward-looking crystals
Downward Shielding	6 mm thick lead plate is used for downward-shielding
Spectra	Collected spectra of 256/512 channels, internal spectrum resolution 1024
Software	Calibration: High voltage adjustment, linearity correction coefficients calculation, and communication test support Real Time Data Collection: Automatic Gain real time control on natural isotopes, and PC based test and calibration software suite
Sensor	Each box containing two (2) gamma detection NaI(Tl) crystals – each 4.2 litres. (256 cu in.) (approx. 100 x 100 x 650 mm) Total volume of approx 8.4 litres or 512 cu in with detector electronics
Spectra Stabilization	Real time automatic corrections on radio nuclei: Th, U, K. No implanted sources

Pico Envirotec AGIS data recorder system Specifications

(for navigation and geophysical data acquisition)

Functions	Airborne Geophysical Information System (AGIS) with integrated Global Positioning System Receiver (GPS) and all necessary navigation guidance software. Inputs for geophysical sensors - portable gamma ray spectrometer GRS-10/AGRS, MMS4 Magnetometer, Totem 2A EM, A/D converter, temperature probe, humidity probe, barometric pressure probe, and laser altimeter. Output for the multi-parameter PGU (Pilot Guidance Unit)
Display	Touch screen with display of 800 x 600 pixels; customized keypad and operator keyboard. Multi-screen options for real-time viewing of all data inputs, fiducial points, flight line tracking, and GPS channels by operator.
GPS Navigation	12 channel, WAAS/SBAS-enabled
Data Sampling	Sensor dependent
Data Synchronization	Synchronized to GPS position
Data File	PEI Binary data format
Storage	80 GB
Supplied Software	PEIView: Allows fast data Quality Control (QC) Data Format: Geosoft GBN and ASCII output PEIConv: For survey preparation and survey plot after data acquisition
Software	Calibration: High voltage adjustment, linearity correction coefficients calculation, and communication test support Real Time Data Collection: Automatic Gain real time control on natural isotopes and PC based test and calibration software suite
Power Requirements	24 to 32 VDC
Temperature	Operating: -10°C to +55°C; storage: -20°C to +70°C

Appendix B

Digital File Descriptions

- Magnetic database description
- Radiometric database description
- Grids
- Maps

Magnetic Database:

Abbreviations used in the GDB/XYZ files listed below:

CHANNEL	UNITS	DESCRIPTION
X_WGS84	m	UTM Easting – WGS 84 Zone 8N
Y_WGS84	m	UTM Northing – WGS 84 Zone 8N
Lon_deg	Decimal degree	Longitude
Lat_deg	Decimal degree	Latitude
Date	yyyy/mm/dd	Dates of the survey flight(s) – Local
FLT		Flight Line numbers
LineNo		Line numbers
STL		Number of satellite(s)
GPSfix		1 = non-differential 2 = WAAS/SBAS differential
GPStime	Hours:min:secs	GPS time (UTC)
Geos_m	m	Geoidal separation
GHead_deg	Decimal degree	Heading of the aircraft
XTE_m	m	Cross track error
Galt	m	GPS height – WGS 84 Zone 8N (ASL)
Lalt	m	Laser Altimeter readings (AGL)
DTM	m	Digital Terrain Model
Sample_Density	m	Linear distance in meters between adjacent measurement locations; sample frequency is 20 Hz
Speed_km_hr	km/hr	Ground speed of aircraft in km/hr
basemag	nT	Base station temporal data
IGRF		International Geomagnetic Reference Field 2015; 12th generation
Declin	Decimal degree	Calculated declination of magnetic field
Inclin	Decimal degree	Calculated inclination of magnetic field
TMI	nT	Total Magnetic Intensity (levelled)
RMI	nT	Residual Magnetic Intensity (levelled)

Radiometric Database:

Abbreviations used in the GDB/XYZ files:

CHANNEL	UNITS	DESCRIPTION
X_WGS84	m	UTM Easting – WGS 84 Zone 8N
Y_WGS84	m	UTM Northing – WGS 84 Zone 8N
Lon_deg	degree	Longitude
Lat_deg	degree	Latitude
Date	yyyy/mm/dd	Dates of the survey flight(s) – Local
FLT		Flight numbers
LineNo		Line numbers
STL		Number of satellite(s)
GPStime	Hours:min:secs	GPS time (UTC)
Geos_m	m	Geoidal separation
GPSFix		1 = non-differential 2 = WAAS/SBAS differential
GHead_deg	degree	Heading of the aircraft
XTE_m	m	Flight line cross distance
Galt	m	GPS height – WGS 84 Zone 8N (ASL)
Lalt	m	Laser Altimeter readings (AGL)
DTM	m	Digital Terrain Model
Sample_Density	m	Linear distance in metres between adjacent measurement locations; sample frequency is 20 measurements per second
Speed_km_hr	km/hr	Ground speed of aircraft in km/hr
BaroSTP_kPa	KiloPascal	Barometric Altitude (Press and Temp Corrected)
Temp_degC	Degrees C	Air Temperature
Press_kPa	KiloPascal	Atmospheric Pressure
COSFILT	counts/sec	Spectrometer - Filtered Cosmic
UPUFILT	counts/sec	Spectrometer – Filtered Upward Uranium
Kcor	%	Equivalent Concentration - Potassium
Thcor	ppm	Equivalent Concentration - Thorium
Ucor	ppm	Equivalent Concentration - Uranium
TCcor	µR	Equivalent Dose Rate
TCexp	µR/hour	Exposure Rate - SUM(%k, eU, eTh) * determined factors
KThratio		Spectrometer –%K/eTh ratio
KUratio		Spectrometer –%K/eU ratio
ThKratio		Spectrometer – eTh/%K ratio
ThUratio		Spectrometer – eTh/eU ratio
UKratio		Spectrometer – eU/%K ratio
UThratio		Spectrometer – eU/eTh ratio

Grids: Golden Horseshoe Survey Block, WGS 84 Datum, Zone 8N, cell size at 25 m

FILE NAME	DESCRIPTION
18106_GoldenHorseshoeBlock_DTM_25m.grd	Digital Terrain Model gridded at 25 m cell size
18106_GoldenHorseshoeBlock_TMI_25m.grd	Total Magnetic Intensity gridded at 25 m cell size
18106_GoldenHorseshoeBlock_RMI_25m.grd	Residual Magnetic Intensity gridded at 25 m cell size
18106_GoldenHorseshoeBlock_CVG_25m.grd	Calculated Vertical Gradient of RMI gridded at 25 m cell size
18106_GoldenHorseshoeBlock_RTP_25m.grd	Reduced to Magnetic Pole of RMI gridded at 25 m cell size
18106_GoldenHorseshoeBlock_CHG_25m.grd	Calculated Horizontal Gradient of RMI gridded at 25 m cell size
18106_GoldenHorseshoeBlock_Kcor_25m.grd	Potassium (%K) - equivalent concentration in percentage gridded at 25 m cell size
18106_GoldenHorseshoeBlock_Thcor_25m.grd	Thorium (eTh) – equivalent concentration gridded at 25 m cell size
18106_GoldenHorseshoeBlock_Ucor_25m.grd	Uranium (eU) – equivalent concentration gridded at 25 m cell size
18106_GoldenHorseshoeBlock_TCcor_25m.grd	Total Count (TCcor) – equivalent dose rate gridded at 25 m cell size
18106_GoldenHorseshoeBlock_TCexp_25m.grd	Total Count (TCexp) – exposure rate gridded at 25 m cell size
18106_GoldenHorseshoeBlock_KThratio_25m.grd	Potassium over Thorium ratio (%K/eTh) gridded at 25 m cell size
18106_GoldenHorseshoeBlock_KUratio_25m.grd	Potassium over Uranium ratio (%K/eU) gridded at 25 m cell size
18106_GoldenHorseshoeBlock_UThratio_25m.grd	Uranium over Thorium ratio (eU/eTh) gridded at 25 m cell size
18106_GoldenHorseshoeBlock_UKratio_25m.grd	Uranium over Potassium ratio (eU/%K) gridded at 25 m cell size
18106_GoldenHorseshoeBlock_ThKratio_25m.grd	Thorium over Potassium ratio (eTh/%K) gridded at 25 m cell size
18106_GoldenHorseshoeBlock_ThUratio_25m.grd	Thorium over Uranium ratio (eTh/eU) gridded at 25 m cell size

Maps: Golden Horseshoe Survey Block, WGS 84 Datum, Zone 8N (jpegs and pdfs)

FILE NAME	DESCRIPTION
18106_GoldenHorseshoeBlock_ActualFlightLines	Plotted actual flown flight lines
18106_GoldenHorseshoeBlock_DTM_25m	Digital Terrain Model gridded at 25 m cell size
18106_GoldenHorseshoeBlock_TMI_wFL_25m	Total Magnetic Intensity gridded at 25 m cell size with plotted actual flown flight lines
18106_GoldenHorseshoeBlock_TMI_25m	Total Magnetic Intensity gridded at 25 m cell size
18106_GoldenHorseshoeBlock_RMI_25m	Residual Magnetic Intensity gridded at 25 m cell size
18106_GoldenHorseshoeBlock_CVG_25m	Calculated Vertical Gradient of RMI gridded at 25 m cell size
18106_GoldenHorseshoeBlock_RTP_25m	Reduced to Magnetic Pole of RMI gridded at 25 m cell size
18106_GoldenHorseshoeBlock_CHG_25m	Calculated Horizontal Gradient of RMI gridded at 25 m cell size
18106_GoldenHorseshoeBlock_Kcor_25m	Potassium (%K) - equivalent concentration in percentage gridded at 25 m cell size
18106_GoldenHorseshoeBlock_Thcor_25m	Thorium (eTh) – equivalent concentration gridded at 25 m cell size
18106_GoldenHorseshoeBlock_Ucor_25m	Uranium (eU) – equivalent concentration gridded at 25 m cell size
18106_GoldenHorseshoeBlock_TCcor_25m	Total Count (TCcor) – equivalent dose rate gridded at 25 m cell size
18106_GoldenHorseshoeBlock_TCexp_25m	Total Count (TCexp) – exposure rate gridded at 25 m cell size
18106_GoldenHorseshoeBlock_KThratio_25m	Potassium over Thorium ratio (%K/eTh) gridded at 25 m cell size
18106_GoldenHorseshoeBlock_KUratio_25m	Potassium over Uranium ratio (%K/eU) gridded at 25 m cell size
18106_GoldenHorseshoeBlock_UThratio_25m	Uranium over Thorium ratio (eU/eTh) gridded at 25 m cell size
18106_GoldenHorseshoeBlock_UKratio_25m	Uranium over Potassium ratio (eU/%K) gridded at 25 m cell size
18106_GoldenHorseshoeBlock_ThKratio_25m	Thorium over Potassium ratio (eTh/%K) gridded at 25 m cell size
18106_GoldenHorseshoeBlock_ThUratio_25m	Thorium over Uranium ratio (eTh/eU) gridded at 25 m cell size
18106_GoldenHorseshoeBlock_TernaryMap_25m	Displaying ratios of all three elements (%K, eTh, eU)

Plates

Golden Horseshoe Survey Block
Scale 1:25,000

- Plate 1: Golden Horseshoe Block - Actual Flight Lines (FL)
- Plate 2: Golden Horseshoe Block - Digital Terrain Model (DTM)
- Plate 3: Golden Horseshoe Block - Total Magnetic Intensity with Actual Flight Lines (TMI_wFL)
- Plate 4: Golden Horseshoe Block - Total Magnetic Intensity (TMI)
- Plate 5: Golden Horseshoe Block - Residual Magnetic Intensity (RMI)
- Plate 6: Golden Horseshoe Block - Calculated Vertical Gradient (CVG) of RMI
- Plate 7: Golden Horseshoe Block - Reduced to Magnetic Pole (RTP) of RMI
- Plate 8: Golden Horseshoe Block - Calculated Horizontal Gradient (CHG) of RMI
- Plate 9: Golden Horseshoe Block - Potassium – Equivalent Concentration in Percentage (%K)
- Plate 10: Golden Horseshoe Block - Thorium – Equivalent Concentration (eTh)
- Plate 11: Golden Horseshoe Block - Uranium – Equivalent Concentration (eU)
- Plate 12: Golden Horseshoe Block - Total Count – Equivalent Dose Rate (TCcor)
- Plate 13: Golden Horseshoe Block - Total Count – Exposure Rate (TCexp)
- Plate 14: Golden Horseshoe Block - Potassium over Thorium Ratio (%K/eTh)
- Plate 15: Golden Horseshoe Block - Potassium over Uranium Ratio (%K/eU)
- Plate 16: Golden Horseshoe Block - Uranium over Thorium Ratio (eU/eTh)
- Plate 17: Golden Horseshoe Block - Uranium over Potassium Ratio (eU/%K)
- Plate 18: Golden Horseshoe Block - Thorium over Potassium Ratio (eTh/%K)
- Plate 19: Golden Horseshoe Block - Thorium over Uranium Ratio (eTh/eU)
- Plate 20: Golden Horseshoe Block - Ternary Map (TM)